

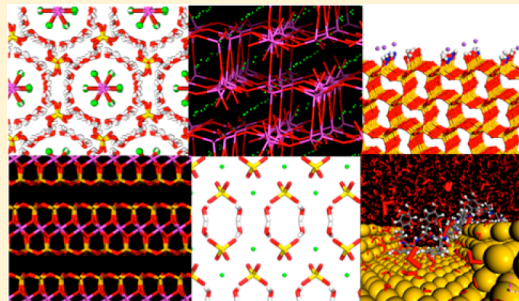
Thermodynamically Consistent Force Fields for the Assembly of Inorganic, Organic, and Biological Nanostructures: The INTERFACE Force Field

Hendrik Heinz,* Tzu-Jen Lin, Ratan Kishore Mishra, and Fateme S. Emami

Department of Polymer Engineering, University of Akron, Akron, Ohio 44325, United States

Supporting Information

ABSTRACT: The complexity of the molecular recognition and assembly of biotic–abiotic interfaces on a scale of 1 to 1000 nm can be understood more effectively using simulation tools along with laboratory instrumentation. We discuss the current capabilities and limitations of atomistic force fields and explain a strategy to obtain dependable parameters for inorganic compounds that has been developed and tested over the past decade. Parameter developments include several silicates, aluminates, metals, oxides, sulfates, and apatites that are summarized in what we call the INTERFACE force field. The INTERFACE force field operates as an extension of common harmonic force fields (PCFF, COMPASS, CHARMM, AMBER, GROMACS, and OPLS-AA) by employing the same functional form and combination rules to enable simulations of inorganic–organic and inorganic–biomolecular interfaces. The parametrization builds on an in-depth understanding of physical–chemical properties on the atomic scale to assign each parameter, especially atomic charges and van der Waals constants, as well as on the validation of macroscale physical–chemical properties for each compound in comparison to measurements. The approach eliminates large discrepancies between computed and measured bulk and surface properties of up to 2 orders of magnitude using other parametrization protocols and increases the transferability of the parameters by introducing thermodynamic consistency. As a result, a wide range of properties can be computed in quantitative agreement with experiment, including densities, surface energies, solid–water interface tensions, anisotropies of interfacial energies of different crystal facets, adsorption energies of biomolecules, and thermal and mechanical properties. Applications include insight into the assembly of inorganic–organic multiphase materials, the recognition of inorganic facets by biomolecules, growth and shape preferences of nanocrystals and nanoparticles, as well as thermal transitions and nanomechanics. Limitations and opportunities for further development are also described.



1. INTRODUCTION

The assembly of inorganic, organic, and biological molecules into functional nanostructures is of interest for a diverse range of applications such as the restoration of human tissue, devices for energy conversion, building materials, nanocomposites, sensors, and catalysis.^{1–7} Observed macroscopic properties are the result of physical and chemical forces on the scale of 1 to 1000 nm, which are often difficult to characterize using available instrumentation. The targeted manipulation of materials using synthesis and characterization techniques, therefore, benefits from added understanding and guidance by modeling, simulation, and theory.

Available simulation techniques comprise methods for specific length and time scales, including quantum mechanical (QM), molecular dynamics (MD), Monte Carlo (MC), field-based, and finite element methods (Figure 1).^{8–10} Each method involves models of chemical species in a defined 3D morphology to understand, for example, reaction mechanisms, molecular recognition, intermolecular forces, self-assembly, morphology preferences, and mechanical properties.^{6,7,11–13} Individual simulation methods have been extensively reviewed, and an overview can be found in section S1 of the Supporting Information. The key to the success of any simulation using electronic structure, all-atom force fields, or coarse-grained

models is the accuracy of the energy expression (Hamiltonian). The energy expression delivers the intermolecular potential, influences the motion of the atoms, and determines the computed thermodynamic properties.^{10,11,14} It is thus the major assumption to ensure the correlation of simulation results with laboratory measurements.

This article summarizes atomistic force fields for inorganic compounds that have been integrated into biomolecular- and materials-oriented force fields and enable the accurate simulation of organic–inorganic and biomolecular–inorganic interfaces on a scale of 1 to 1000 nm. The strengths and weaknesses of current atomistic force fields, motivations for the development of parameters for inorganic compounds, and conceptual improvements are discussed in section 2. The thermodynamically consistent interpretation and derivation of force field parameters is described in section 3. Validation, examples, and limitations for the simulation of bulk materials, surfaces, and interfaces are presented in section 4, followed by conclusions and perspectives in

Received: June 1, 2012

Revised: December 30, 2012

Published: December 31, 2012

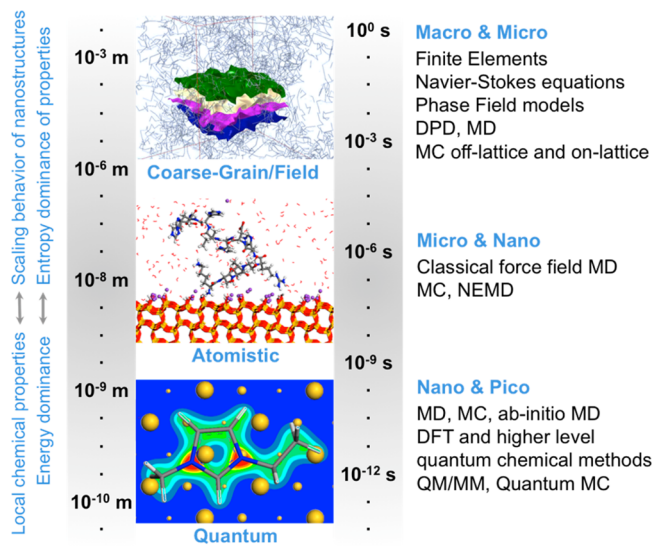


Figure 1. Simulation techniques with associated length and time scales (diagrammatic style similar to that in Praprotnik et al.⁹).

section 5. Specific details and additional references are provided in the Supporting Information.

2. FORCE FIELDS FOR INORGANIC COMPOUNDS

2.1. Motivation. Current simulation studies attempt to solve problems across a broad range of topics related to energy science, medicine, electronics, composites, catalysis, and bioengineering using essentially the same set of computational tools. (See section S2.1 for a survey of interface simulations.) Force fields are a critical workhorse for such calculations on the length scale of 1 to 1000 nm. The arguably oldest force fields were developed by Max Born in the form of constants for Coulomb attraction and exponential repulsion¹⁵ as well as by S. E. Jones as exponential $n-m$ Lennard-Jones potentials.^{16,17} Harmonic energy expressions containing more detail have been developed with the emergence of computer power since the 1980s. Harmonic energy expressions include AMBER,¹⁸ CHARMM,¹⁹ COMPASS,²⁰ CVFF,²¹ DREIDING,²² GROMACS,^{23,24} MMFF,²⁵ OPLS-AA,²⁶ PCFF,²⁷ TEAMFF (a recent development by Huai Sun's group), and TraPPE.²⁸ These force fields reproduce many properties of proteins, carbohydrates, DNA, solvents, drug molecules, surfactants, and polymers in good agreement with experiment. Besides, more specialized force fields have been developed, such as Buckingham potentials for certain minerals and polymers,^{29–32} EAM models for metals,³³ ReaxFF to simulate chemical reactions,³⁴ bond-order potentials for semiconductors and hydrocarbons (Tersoff, AIREBO),^{35–37} and the AMOEBA force field for polarizable models (Figure 2).³⁸ These

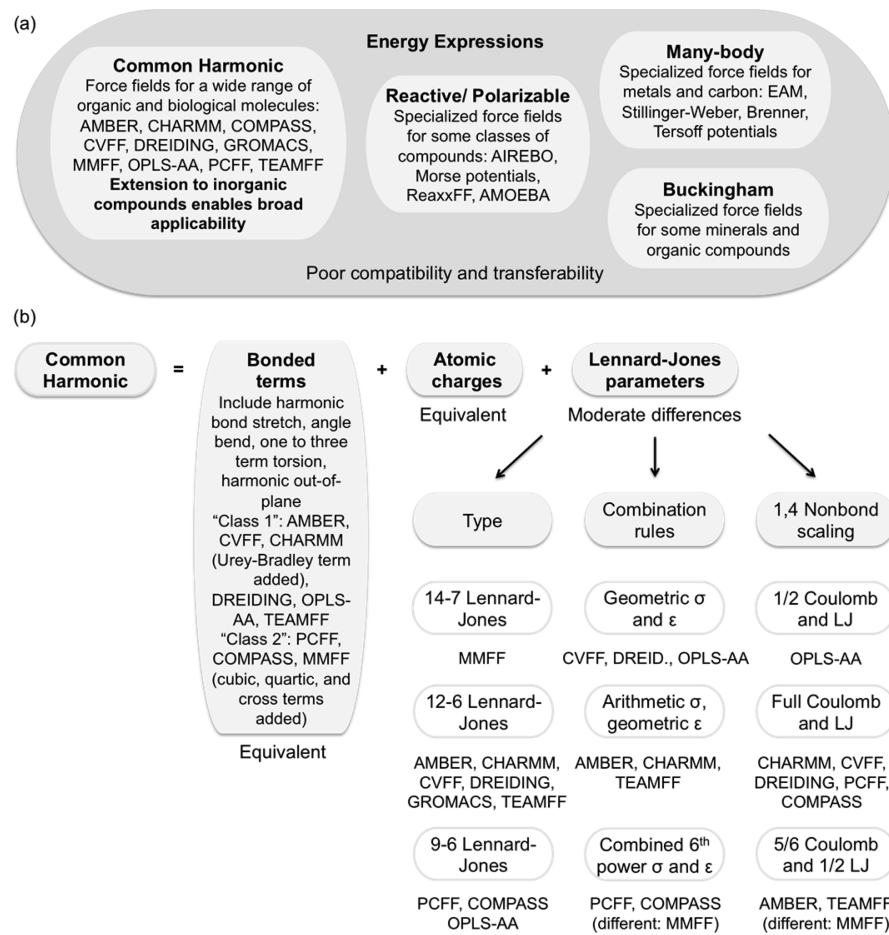


Figure 2. Available force fields and challenges in transferability. (a) Parameters of different energy expressions can hardly be processed into a uniform force field for both organic and inorganic components. (b) Harmonic energy expressions such as AMBER, CHARMM, OPLS-AA, and PCFF are similar and contain quality parameters for organic compounds. Bonded terms and atomic charges for newly added compounds are physically identical. Moderate differences in the type of Lennard-Jones (LJ) potential, combination rules, and the scaling of nonbonding interactions between 1,4-bonded atoms (1,4 nonbond scaling) can be overcome by adjustments of $\sigma_{0,ii}$ and $\epsilon_{0,ii}$ to reproduce closely the same bulk and interfacial properties.

Table 1. Summary of Compounds Parameterized in the INTERFACE Force Field and Examples of Validation under Standard Conditions^a

compound	property	experiment	INTERFACE force field	other force fields	key refs
1. Layered Silicates: Mica, Montmorillonite, and Pyrophyllite					
any in this group	average deviation of cell parameters ($a, b, c, \alpha, \beta, \gamma$) and density (ρ) from experiment	$\pm 0.1\%$	$\pm 0.5\%$	1–5%, often amorphization	13, 14, 76
mica	cleavage energy {001} (mJ/m ²)	375	380	–400 to +700	14, 49
	surface tension, alkyl-modified (mJ/m ²)	41–46	45 ± 3	NA	49, 50, 66
pyrophyllite	surface tension $\gamma = \gamma^{\text{el}} + \gamma^{\text{vdW}}$ (mJ/m ²)	39.7 ± 1	40 ± 1	–1000 to +260	14
	electrostatic contribution γ^{el} (mJ/m ²)	5.8 ± 1	8 ± 1	2–155	14
	van der Waals contribution γ^{vdW} (mJ/m ²)	33.9 ± 1	32 ± 1	–1100 to +250	14
2. Silicates and Aluminates in Cement: Tricalcium Silicate, Tricalcium Aluminate, Ettringite, 11 and 14 Å Tobermorites, and Monosulfate					
any in this group	average deviation of cell parameters ($a, b, c, \alpha, \beta, \gamma$) and density (ρ) from experiment	$\pm 0.1\%$	$\pm 0.5\%$	NA	47, 48
tricalcium silicate	cleavage energy (mJ/m ²)	1300 ± 100	1340 ± 20	NA	47, 48, S14
	bulk modulus (GPa)	105.2 ± 5	105 ± 2	NA	47, 48, S14
tobermorite 11 Å	water interfacial tension {100} (mJ/m ²)	10–50	34 ± 5	NA	48
tobermorite 14 Å	facet-averaged surface energy (mJ/m ²)	390 ± 20	390 ± 10	NA	48, S15
	bulk modulus (GPa)	15 ± 2	15 ± 1	NA	48, S14
3. FCC Metals: Ag, Al, Au, Cu, Ni, Pb, Pd, and Pt					
any in this group	average deviation of cell parameters ($a, b, c, \alpha, \beta, \gamma$) and density (ρ) from experiment	$\pm 0.01\%$	$\pm 0.1\%$	0–5%	40
gold	surface tension γ_{SV} {111} (mJ/m ²)	1540	1540 ± 5	1000–3000	40
	water interfacial tension γ_{SL} {111} (mJ/m ²)	1470	1350 ± 10	1000–3000	40, 51
	anisotropy $\gamma\{100\}/\gamma\{111\}$	1.04 ± 0.01	1.035 ± 0.01	1.03–1.07	40
	anisotropy $\gamma\{110\}/\gamma\{111\}$	1.10 ± 0.02	1.10 ± 0.02	1.08–1.20	40
	strongest-binding amino acids to {111}	R, W, Y	R, W, N	Y, F, H, or NA	52–54
palladium (with 12–6 LJ)	Young's modulus (GPa)	146 ± 1	146	90–240	40
	bulk modulus (GPa)	193 ± 1	182	120–280	40
	shear modulus (GPa)	53.2 ± 0.5	53	30–90	40
	specific molecular binding to {111}/{100}	yes	yes	NA	52, 55
4. Silica: Bulk and Q⁴, Q³, and Q² Surfaces with Different Ionization (Representing Different Particle Sizes, pH, and Hydration)					
quartz	average deviation of cell parameters ($a, b, c, \alpha, \beta, \gamma$) and density (ρ) from experiment	$\pm 0.1\%$	$\pm 1\%$	0–5% or amorphization	7
Q ³ silica surface	immersion energy in water (mJ/m ²)	–160 ± 5	–167 ± 5	–50 to –500	7, 48, S16
	water contact angle at zero charge (deg)	0	0	0–50	7, 48
	adsorption energy of selected peptides at 20% ionization in water (kcal/mol)	–4 to –6	–4 to –6	no ionization considered	7, 48
Q ⁴ silica surface	water contact angle (deg)	42 ± 2	42 ± 3	0–50	48, S16
5. Sulfates and Phosphates: Gypsum, Plaster of Paris, and Hydroxyapatite					
any in this group	average deviation of cell parameters ($a, b, c, \alpha, \beta, \gamma$) and density (ρ) from expt	$\pm 0.1\%$	$\pm 0.5\%$	0–5% or NA	47, 48
gypsum	facet-averaged surface tension (mJ/m ²)	370 ± 10	355 ± 10	300–1000	47, 48, S17
	facet-averaged water interface tension (mJ/m ²)	64 ± 1	67 ± 3	50–200	47, 48, S17
hydroxyapatite	cleavage energy {001} (mJ/m ²)	800–900	860 ± 10	–500 to +3000	48, S18
	bulk modulus (GPa)	87 ± 2	79 ± 3	60–110	48

^aA selection of key properties is shown for every group of compounds, including measurement, computation using the INTERFACE force field, and computation with alternative force fields, if available. The full spectrum of validated properties for every compound can be retrieved from the key references that contain all of the following: specific references for experimental data, an exhaustive list of computed properties using the INTERFACE force field (then called differently), and comparisons to alternative force fields. Because every compound of more than twenty was validated individually in detail, space limitations in this article do not allow the listing of all original references and data.

specialized energy expressions are typically more limited in transferability, restricted to a narrower range of compounds, and involve a larger number of parameters.

In contrast to the availability and quality of parameters for organic molecules, force fields for inorganic compounds such as silicates, aluminates, oxides, and metals are often not available or exhibit large deviations relative to known surface properties. In particular, computed interfacial properties such as hydration energies, surface

tensions, and adsorption energies may depart by multiples from measurements.^{14,20,21,27,29–32,39–46} pH equilibria and other details of surface structures have been frequently disregarded, and some models require fixed atom positions during simulation to avoid shrinkage or amorphization. In addition, the simulation of organic–inorganic and biomolecular–inorganic interfaces is hardly possible when the energy expressions for inorganic and organic compounds are dissimilar (i.e., with many of the specialized force fields, Figure 2a).

We explain a convenient solution, the INTERFACE force field, that overcomes these challenges and enables the accurate simulation of inorganic compounds, biomolecules, and polymers using a single platform. The INTERFACE force field is a collection of all-atom parameters for inorganic compounds that have individually undergone extensive validation, reproduce a multitude of bulk and surface properties in excellent agreement with measurements, and reduce deviations from experimental data by up to 2 orders of magnitude compared to alternative force fields. The parametrization builds on an in-depth understanding of physical–chemical properties on the atomic scale to assign each parameter as well as on the validation of macroscale physical–chemical properties for each compound in comparison to measurements. The parameters employ the same harmonic energy expressions as existing parameters for biomolecules, solvents, and polymers using standard combination rules (Figure 2b and the INTERFACE-PCFF force field in the Supporting Information).

More than 20 common minerals, metals, and poly(ethylene oxide) are currently included (Table 1 and Figure S1). Parameters were initially developed for clay minerals,¹⁴ followed by cement minerals (unpublished for many years),^{47,48} fcc metals,⁴⁰ silica,^{7,48} sulfates,⁴⁷ and recently phosphates.⁴⁸ Most of these developments were individually reported and extensively tested as part of various platforms (PCFF, CVFF, and CHARMM). Parameters for some cement minerals, PEO, and apatites are newly included here, and validation in detail will be reported separately.

2.2. Choice of Energy Expression. The use of distinct energy expressions for inorganic compounds versus organic compounds is often a roadblock to simulating inorganic–organic interfaces (Figure 2a). Harmonic energy expressions are promising for extension to inorganic compounds because of the analogy to quantum mechanical models and available parameters for biomolecules and polymers of good quality (Table 2, Figure 2a). In contrast, Buckingham potentials for minerals^{29–31} are difficult to combine with harmonic expressions for proteins, carbohydrates, and DNA (e.g., AMBER and CHARMM). Embedded atom potentials for metals are of an entirely different functional form and are very difficult to combine with force fields for polymers and biomolecules.³³ The same is true for bond-order potentials.^{35–37} The energy expression for reactive force fields such as ReaxFF includes very complex bond-order terms and customized corrections³⁴ that cannot be merged with or extend known harmonic energy expressions. Polarizable force fields such as AMOEBA also require specialized parametrization.³⁸ Parameters for inorganic compounds using simple, interpretable harmonic energy expressions are therefore a good starting point for a uniform force field and are possibly extensible to reactive and other specialized energy expressions.

Differences of a lesser extent are also found among the harmonic force fields (Figure 2b). Parameters for a new compound in one force field cannot be used in another if there are changes in the type of Lennard-Jones potential, changes in combination rules, and changes in the scaling of nonbonding interactions between 1,4-bonded atoms (1,4 nonbond scaling). The force field for an inorganic compound must then be recast in the form of another harmonic force field by making changes in van der Waals parameters ($\sigma_{ii,0}$, $\epsilon_{ii,0}$) and torsion parameters ($V_{\varphi_{n,ijkl}}$, $\varphi_{0n,ijkl}$) and via minor additional testing. For example, (1) a change in combination rules for 12–6 LJ potentials only (e.g., CVFF to CHARMM) may not require any, or very minor, adjustments, (2) changes in the LJ potential with the same scaling of nonbonding interactions between 1,4-bonded atoms (e.g., PCFF to CHARMM) require adjustments in LJ parameters and in torsion parameters, and (3) changes in the

Table 2. Impact of Force Field Parameters in All-Atom Simulations of Inorganic–Organic Interfaces in Decreasing Order^a

parameter	impact on simulation
compatibility of parameters with existing force fields for (bio)organic compounds	scope of application
atomic charges	surface and interface properties, adsorption, conformation of polar molecules
Lennard-Jones well depth	surface and interface properties, adsorption, cohesion, conformation of molecules
surface chemistry (hydration, protonation, charge defects)	interfacial properties and dynamics
torsion potential	molecular conformation, chain folding
Lennard-Jones diameter ^b	density (atom size)
vibrational constants	IR/Raman spectra, elastic properties
bond and angle constants ^c	geometry of covalent bonds and angles

^aThe list focuses on polar inorganic compounds with high sensitivity to atomic charges and also applies to organic compounds that are usually of lower polarity. ^bKnown in good approximation across the periodic table (refs 60 and 61) and necessary refinements for charged atoms using known relationships between electron configuration, ionization state, and ion diameter are straightforward. Adjustments on the order of $\pm 5\%$ to reproduce the density of a compound are acceptable. ^cInitially known from X-ray or neutron diffraction as an important foundation for the model.

scaling of nonbonding interactions between 1,4-bonded atoms for the same type of LJ potential (e.g., OPLS-AA to CHARMM) require adjustments in both LJ parameters and in torsion potentials (if 1,4-bonded atoms are present in the compound).

If one and the same energy expression would be used for all compounds, then adjustments of this nature would no longer be necessary.

2.3. Common Harmonic Energy Expressions. The implementation of thermodynamically consistent force fields for all types of compounds relies on harmonic energy expressions such as those used in CHARMM¹⁹ (eq 1) and PCFF²⁷ (eq 2):

$$\begin{aligned} E_{\text{pot}} = & \sum_{ij \text{ bonded}} K_{r,ij}(r_{ij} - r_{0,ij})^2 + \sum_{ijk \text{ bonded}} K_{\theta,ijk}(\theta_{ijk} - \theta_{0,ijk})^2 \\ & + \sum_{ijkl \text{ bonded}} \frac{1}{2} V_{\varphi,ijkl}[1 + \cos(n\varphi_{ijkl} - \varphi_{0,ijkl})] \\ & + \sum_{ijkl \text{ bonded} \atop (\text{in plane})} K_{\chi,ijkl}(\chi - \chi_{0,ijkl})^2 + \frac{1}{4\pi\epsilon_0\epsilon_r} \sum_{ij \text{ nonbonded} \atop (1,2 \text{ and } 1,3\text{excl})} \frac{q_i q_j}{r_{ij}} \\ & + \sum_{ij \text{ nonbonded} \atop (1,2 \text{ and } 1,3\text{excl})} \epsilon_{0,ij} \left(\left(\frac{r_{0,ij}}{r_{ij}} \right)^{12} - 2 \left(\frac{r_{0,ij}}{r_{ij}} \right)^6 \right) + E_H \end{aligned} \quad (1)$$

$$\begin{aligned} E_{\text{pot}} = & \sum_{ij \text{ bonded}} \sum_{n=2}^4 K_{rn,ij}(r_{ij} - r_{0,ij})^n + \sum_{ijk \text{ bonded}} \sum_{n=2}^4 K_{\theta n,ijk}(\theta_{ijk} - \theta_{0,ijk})^n \\ & + \sum_{ijkl \text{ bonded}} \sum_{n=1}^3 V_{\varphi n,ijkl}[1 - \cos(n\varphi_{ijkl} - \varphi_{0n,ijkl})] \\ & + \sum_{ijkl \text{ bonded} \atop (\text{in plane})} K_{\chi,ijkl}(\chi - \chi_{0,ijkl})^2 + E_{\text{cross}} + \frac{1}{4\pi\epsilon_0\epsilon_r} \sum_{ij \text{ nonbonded} \atop (1,2 \text{ and } 1,3\text{excl})} \frac{q_i q_j}{r_{ij}} \\ & + \sum_{ij \text{ nonbonded} \atop (1,2 \text{ and } 1,3\text{excl})} \epsilon_{0,ij} \left(2 \left(\frac{r_{0,ij}}{r_{ij}} \right)^9 - 3 \left(\frac{r_{0,ij}}{r_{ij}} \right)^6 \right) \end{aligned} \quad (2)$$

The total potential energy of the simulation system depends only on the Cartesian coordinates of the atoms and contains contributions from intramolecular (bonded) interactions as well as from intermolecular (nonbonded) interactions. The potential energy of class I force fields contains additive terms for a quadratic bond stretching potential, a quadratic angle bending potential, a trigonometric torsion potential, a quadratic out-of-plane potential, Coulomb interactions, van der Waals interactions, and hydrogen bonds (AMBER,¹⁸ CHARMM,¹⁹ CVFF,²¹ DREIDING,²² and OPLS-AA,²⁶ eq 1). The term E_H for hydrogen bonds is shown only for historical reasons because hydrogen bonds can be well described as a superposition of Coulomb and van der Waals interactions (AMBER, CHARMM, CVFF, and OPLS-AA). Class II force fields include additional cubic and quartic bonded terms as well as cross terms compared to those in class I force fields (COMPASS,²⁰ MMFF with 14–7 LJ,²⁵ and PCFF,²⁷ eq 2). The extra terms can be disregarded for the addition of parameters of new compounds.^{11,56}

2.4. Thermodynamic Consistency. The unavailability of coherent and reliable force fields for inorganic compounds has been related to difficulties in the derivation of nonbonding parameters (i.e., atomic charges q_i , van der Waals diameters $\sigma_{0,ii}$, and well depths $\varepsilon_{0,ii}$). Automated QM and other approaches lead to high scatter in atomic charges q_i that may disagree with trends in electronegativity and basic chemical knowledge. The assignment of well depths $\varepsilon_{0,ii}$ for specific LJ parameters (section 2.2) has also often been a fitting process with limited physical rationale. Because of the number of force field types and parameters, a meaningful parametrization is then hardly feasible, and an incomplete understanding and interpretation of nonbonding parameters is the main reason for disagreement between computed and measured surface properties up to multiples (Table 1).^{14,20,21,27,29–31,39–46} Moreover, restrictions of the mobility of surface atoms have been invoked to avoid instant deformation when force fields were not adequate to simulate stable bulk and surface structures. These approximations do not relieve deficiencies in bulk and interfacial properties and introduce a temperature of absolute zero to the fixed surface.⁵⁷ The surface chemistry of parametrized compounds has often been disregarded. Misrepresentations include the neglect of hydration and protonation equilibria of silica, titania, and apatite surfaces, the type of Miller planes { hkl } displayed on nanostructures, and area densities of defects and cations.

The key to quantitative correlations with measurements and the maximum quality of the force field lies in understanding all parameters in the energy expression (Table 2).¹⁴ An advantage of harmonic force fields over other models (e.g., QM basis sets, density functionals, ReaxFF, AIREBO, and EAM models) is a smaller number of parameters and the feasibility to assign a quantitative meaning to each parameter in the context of corresponding experimental and theoretical measures. Thermodynamic consistency is achieved by in-depth analysis and testing of the parameters by the comparison of individual force field parameters to atomic-scale experimental quantities (atomic charges, dipole moments, and torsion barriers) and aggregate computed properties to aggregate observables (cell parameters, surface tension, hydration energy, and elastic moduli). Once every compound is parametrized in this way, combination rules of Lennard-Jones parameters provide interaction parameters between different atom types in the same compound and between atom types in different compounds of good quality, for example, between biomolecules and solvents,^{18–23,25–27} inorganic surfaces and solvents, and inorganic surfaces and

biomolecules (section S3). Each compound in the INTERFACE force field provides evidence that the interpretation and assignment of parameters consistent with known chemical and physical properties eventually lead to the best possible performance.

Thermodynamic consistency builds on two major concepts (Figure 3). First, atomic charges can be consistently derived on the basis of measured electron deformation densities, dipole moments, dielectric constants, and electrostatic contributions to the surface tension for a wide range of inorganic compounds (Figure 3a).⁵⁸ The retroactive computation of such data using the atomic charges in a force field demonstrates the high sensitivity to deviations in atomic charges.^{14,47,49,58} Second, once atomic charges agree with observable physical–chemical properties, the examination of computed cleavage energies, surface tensions, hydration energies, and solid–liquid interface tensions in comparison to laboratory measurements (refs 59 and S14–S18) is equally important in adjusting initial van der Waals parameters (Figure 3b).^{7,14,40,47,49,50} The corresponding refinement of van der Waals parameters, particularly well depths $\varepsilon_{0,ii}$, ensures accurate computed interfacial properties and enables the physical interpretation of the parameters. This is especially encouraged because valuable laboratory data for many minerals and crystal facets have become available over the last century (refs 59 and S14–S18). Thermodynamic consistency of the parameters then also enables the computation of adsorption energies of organic and biological molecules in agreement with experiment, given the same parameter quality for inorganic and organic compounds. As a third concept, all other bonded terms in the force field are chosen to correspond to their physical equivalents, whereby inorganic compounds often require bond and angle terms only.¹¹

This approach, as first applied to mica-type silicates, has led to accurate parameters for a range of minerals (Table 1, Figure S1). Key characteristics are (1) the quantitative reproduction of bulk and surface properties, such as computed cell parameters, surface energies, and thermal and mechanical properties with an increase in accuracy up to 2 orders of magnitude over earlier parameters, (2) integration in harmonic force fields such as AMBER, CHARMM, PCFF, COMPASS, and OPLS-AA, and (3) the ease of extension to new compounds and a high level of transferability due to a limited number of parameters with clearly identified physical meaning. The INTERFACE force field summarizes the parameters and functions as a plug-in to a harmonic force field (e.g., INTERFACE-PCFF, INTERFACE-CHARMM) to enable simulations of inorganic compounds, biomolecules, and polymers using a single platform.

3. DERIVATION OF PARAMETERS

The derivation of parameters is described in detail in the Supporting Information (Figure S2 and section S4). We focus here on the most critical approaches that set the developments apart from other parametrizations and lead to the reported improvements in computed properties (Table 1). The protocol works regardless of the type of compound (e.g., metal, mineral, or polymer).

3.1. Definition of Atom Types. The first step in the derivation of force field parameters is the examination of a crystal structure from X-ray data, if available, or the 3D chemical formula to determine the number of atom types that represent bonded and nonbonded interactions (Figure S2). This step defines the resolution of the force field and involves at least one atom type for each element in a given compound, plus possible additional

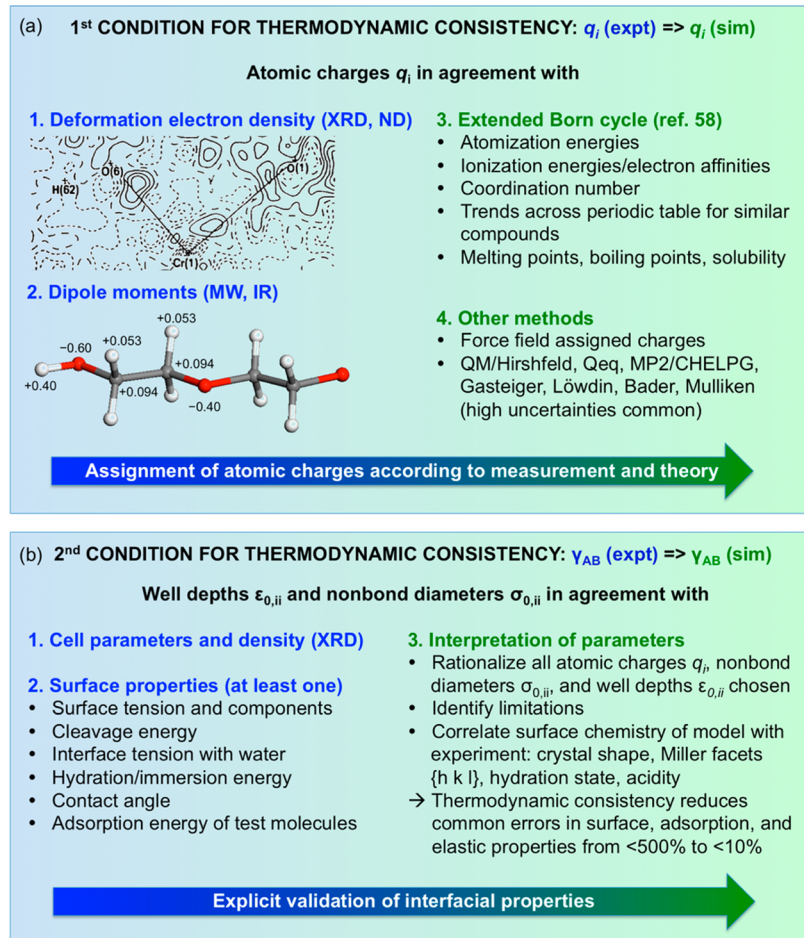


Figure 3. Most important criteria for obtaining thermodynamically consistent force field parameters. (a) Atomic charges and (b) computed interfacial properties in the models should quantitatively agree with atomic-scale and macroscale experimental data. The color scheme and single-headed arrows emphasize the feed of information from experiment (blue) into models and theory (green).

atom types for the same element in different chemical environments, similar to the distinction of chemical environments by NMR methods. For example, oxygen possesses different atom types in phosphate, hydroxide, silanol, and ether groups.

Some atom types of the same element can be very similar in different compounds and are regarded as identical in the force field. Others can be somewhat similar, but their distinction notably improves the quality of the force field, for example, Si and O in silicate rings versus silicate ions. In some compounds, extra atom types are needed to parametrize chemically unique bonds, angles (e.g., clay minerals), torsions, or van der Waals interactions. The number of atom types in the INTERFACE force field aims at a chemically reasonable minimum and amounts to about 70 atom types for 30 different compounds.

The resolution of the force field could in principle be changed, for example, (1) by the choice of multiple atom types per atom to depict lone pairs and other details of electronic structure in addition to the nucleus position, which would lead to polarizable force fields, or (2) by the choice of atom types that represent complete functional groups or entities composed of several atoms, which would lead to coarse-grained models (Figure 1). Any such changes would require new parametrization efforts.

3.2. Atomic Charges. The foremost important parameters are atomic charges q_i because they reflect the electron density in the compound (Figure 3a).⁵⁸ We accumulated extensive evidence, since the publication of ref 58, that experimental

insight and chemical understanding lead to justified atomic charges for simulations. The atomic charges can be derived in multiple ways with a high level of convergence to the same values, and only then, knowing the remaining uncertainty, are the charges accepted for the force field. The sources of atomic charges include (1) experimental measurements of deformation electron densities (Table S1, refs S19–S25), (2) measured dipole moments,⁶⁰ (3) the extended Born thermodynamic cycle including an analysis of covalent and ionic bonding contributions,⁵⁸ (4) the influence of coordination numbers and the aggregate state of a given compound on atomic charges, (5) the relationship of atomic charges to melting points, solubility, and cleavage energies for a set of similar compounds with similar degrees of covalent bonding, (6) the relationship of atomic charges to chemical reactivity and reaction mechanisms for similar compounds reported in the literature, and (7) the relationship between chemical structure and atomic charges for comparable compounds with known atomic charges across the periodic table.⁵⁸

The discussion of individual compounds in the INTERFACE force field in prior work has always shown convergence in atomic charges (i.e., a high level of consistency between the assigned degree of polarity and the above-mentioned physical–chemical properties^{7,14,47–50}). The resulting uncertainty in atomic charges q_i is $\pm 0.1e$ to $\pm 0.2e$ for highly charged compounds and <10% for compounds with atomic charges below $\pm 1.0e$. Often, the application of one or two of the above concepts leads to very

good values q_i , especially when taking into account a growing library of experimental benchmark compounds (Table S1) and compounds with tested force fields (molecular models in the Supporting Information).

The closest equivalent QM methods used to derive atomic charges for molecular simulations are computations of the electron density at a high level of theory in combination with Hirshfeld partitioning of the charge density into approximately spherical atomic basins.⁶² This approach can yield dipole moments as well as Coulomb contributions to cleavage energies and surface tensions, in good agreement with measurements. The Hirshfeld method is also the preferred method of partitioning electron deformation densities from laboratory measurements. Nevertheless, the accuracy of the electron density calculated by QM methods appears to be lower as in the experiment. QM methods also require a consideration of the correct aggregate state, and particular difficulties arise for electron densities of elements with d and f electrons. Because atomic charges often reflect minor differences in the total electron density, deviations up to multiples compared to the real system may occur. Besides, different partitioning schemes such as that by Mulliken or by Bader can lead to additional overestimates in atomic charges by over 30% compared to Hirshfeld charges (ref S26). Uncertainties of up to several hundred percent have also been reported for Löwdin charges, MP2/CHELPG charges, and M06-derived charges.^{10,58,63} Unexpected atomic charges are very difficult to explain and invalidate the entire force field if accepted. Overall, ab initio studies today suggest atomic charges with uncertainties up to multiples^{58,63} and available laboratory measurements since the 1950s quantify atomic charges consistent with known physical chemical properties within a range of $\pm 5\text{--}10\%$ (refs S19–S25). The possible high uncertainty and limited correlation of QM-derived charges with observable properties are the main reasons that we rely on experimental measurements and readily available information about the extent of covalent versus ionic bonding across the periodic table for the assignment of atomic charges, including the extended Born thermodynamic cycle and chemical knowledge (further details in section S4.2).

3.3. Cohesive and Interfacial Properties. The second most important parameters in reproducing interfacial and cohesive properties are the nonbonding diameters $\sigma_{0,ii}$ and, in particular, well depths $\varepsilon_{0,ii}$ (Figure 3b). Their roles consist of the reproduction of atomic volumes and the allocation of dispersive van der Waals contributions to cohesive energies, cleavage energies, surface energies, hydration energies, and other interfacial interactions. These parameters are as important as atomic charges q_i but are always derived second because (1) they would change for a different polarity q_i and (2) remaining inconsistencies in atomic charges would inevitably lead to thermodynamic inconsistency in the force field. The numerical values of $\sigma_{0,ii}$ and $\varepsilon_{0,ii}$ also depend on the type of LJ potential, the scaling rules for nonbonding interactions between 1,4-bonded atoms, and the chemical environment of particular functional groups. These dependencies are difficult to account for by automated procedures when the aim is a force field of physical–chemical consistency, interpretability, and the best possible accuracy.

To proceed with the parametrization, it is best to choose one energy expression to begin with (atomic charges are independent of this choice) and assign trial values of $\sigma_{0,ii}$ and $\varepsilon_{0,ii}$ for each atom type. The trial values of $\sigma_{0,ii}$ follow known van der Waals (or ionic) diameters across the periodic table.^{60,61} The basis for an initial well depth $\varepsilon_{0,ii}$ of an atom i is the polarizability, analogies across the periodic table, and the chemical environment: (1) The

approximate range of $\varepsilon_{0,ii}$ values in a given row of the periodic table is identified according to known $\varepsilon_{0,ii}$ values for rare gases (Halgrens rule).⁶⁴ (2) Changes in the polarizability of each atom according to the charge state are taken into account (e.g., an increase in $\varepsilon_{0,ii}$ for negatively charged atoms). (3) The average number of close nonbonding neighbors (including 1,4-bonded atoms) per unit volume affects the value of $\varepsilon_{0,ii}$ for otherwise similar atoms. This number of neighbors decreases and $\varepsilon_{0,ii}$ increases depending on whether the atom is part of a covalently bonded framework, part of a surface, or an isolated ion. (4) For some polar atoms or ions, an increase in $\varepsilon_{0,ii}$ may also be required to strengthen the repulsive part of the potential through a deeper potential well (details in section S4.3).

Upon the usually less involved assignment of bonded parameters from X-ray data (section S4.4), the initial force field is subjected to a rigorous comparison of computed densities, cleavage energies, hydration energies, and cohesive energies (not in the case of covalent networks) to experimental values under standard conditions using MD simulation in NPT and NVT ensembles. The values of well depths $\varepsilon_{0,ii}$ require the most attention and fine tuning to match experimental surface and bulk properties. These changes along with an interpretation of all parameters yield the final force field. Once the essential bulk and surface properties quantitatively agree, the evaluation can be further extended to surface energy anisotropy and thermal and mechanical properties, which are then typically found to be in good agreement with measurements without further changes.

The subsequent transcription of force field parameters to different harmonic energy expressions (e.g., PCFF to AMBER) involves only adjustments of van der Waals parameters and torsion potentials (if present), followed by rechecks of densities, cleavage energies, hydration energies, and cohesive energies (details in section S4.6). Examples of conversions of LJ parameters are given in refs 14, 40, 47, and 48.

In summary, we rely on the interpretation and validation of each parameter in the context of available physical–chemical data rather than automation. The force field contains no freely adjustable parameters besides a certain range for the well depths $\varepsilon_{0,ii}$. Consequently, the parameters are essentially determined under standard conditions. Further developments may include temperature- and pressure-dependent changes when far from standard conditions (298 K and 101 kPa), extensions for polarizability, adaptation to chemical reactions using Morse and other dedicated potentials, and refinements of combination rules.

3.4. Scope of Use. Parameters in the INTERFACE force field were developed and validated individually for each compound. Therefore, the force field is intended for compounds included in the data set and interfaces with any other compounds that possess thermodynamically consistent parameters. The force field does not aim to provide universal parameters for new compounds, which could lead to a loss of accuracy. Parameters for novel compounds with or without known experimental data can be obtained using the above procedure and helpful benchmarks from existing compounds (details in Figure S2 and section S4.7).

4. VALIDATION, EXAMPLES, AND LIMITATIONS

The INTERFACE force field performs exceptionally well in comparison to experimental data and alternative force fields (Table 1, Figure S1). The validation for each compound is described along with parameter development in separate publications and in publications in progress.^{7,11,13,14,40,47–55,65–67} Contributions to validation and application have also been reported by numerous

research groups, especially for layered silicates and fcc metals for which parameters have been known for some time (section S5 and refs S63–S87). In this section, we provide a representative summary, highlight example problems that have been solved, and describe limitations.

4.1. Accuracy of Bulk and Surface Properties. Computed cell parameters and densities of crystal structures for all compounds exhibit very small deviations from X-ray data, typically as low as 0.2 to 1.0% during NPT dynamics (Table 1). Small deviations for a wide range of chemistry and symmetry (Figure S1) are a strong indicator of the chemical consistency of the force field. Alternative models exhibit typical deviations of 1 to 5% from measurements and sometimes achieve no stable crystal structure at all, requiring artificially frozen surfaces. The INTERFACE force field fully resolves these limitations.

Surface properties including surface tensions, hydration energies, and surface energy anisotropies of all compounds deviate 0 to 10% from experiment (Table 1). Surface properties are a stress test for the quality of a force field because they are more sensitive to parametrization than densities. Many other force fields and even some density functionals fail in this category and exhibit up to 500% deviation. (As explained in section 3, such deviations are related to inconsistent nonbonding parameters. It is not possible to compensate for poor atomic charges with automatically fitted LJ parameters and still obtain both densities and surface properties in agreement with experiment.) Specifically, we note that computed surface energies and surface energy anisotropies of metal {111}, {100}, and {110} facets match experiment more closely than EAM models³³ and some QM models.^{68–70} Excellent agreement is also found for hydration energies of nonreactive surfaces, such as experimentally well characterized {010}, {011}, and {120} surfaces of gypsum as well as pyrogenic silica in water. Coulomb and van der Waals contributions to surface tensions have also been measured separately on well-characterized surfaces.⁵⁹ The INTERFACE force field computes such contributions in very good agreement with laboratory data, tested specifically for mica-type minerals, silica, and gypsum (Table 1).^{14,47–50} Other force fields do not compare favorably at this level because of the incomplete interpretation of nonbonding parameters.

The solid–liquid interfacial tension with water (for non-reconstructing surfaces) and the anisotropy of the solid–liquid interfacial tension for different crystal facets deviate 0 to 10% from experiment for all compounds (refs 40, 47, 48, 59, S15, and S17). The sensitivity to different water models such as SPC water and TIP3P water is only 2–4%, and binding energies of biomolecules and polymers in aqueous solution can be quantitatively computed. Solid–liquid interfacial tensions in other force fields deviate between 0 and 500% from experiment, including anisotropies, binding mechanisms, and binding energies of chain molecules.^{14,39,41–48} These deviations correlate with errors in solid–vapor interfacial tensions, and good results for individual compounds are often incidental.

Mechanical and thermal properties usually agree well with experiment (refs 13, 40, 47, 48, and S14). Deviations of computed elastic constants and moduli typically remain less than $\pm 20\%$, unless covalent frameworks with excess of bonded terms are present (section 4.3). This reliability is similar to QM methods. Alternative force fields often depart up to multiples or were specifically fitted to keep deviations under $\pm 10\%$. Deviations in surface properties up to multiples are then common, however, because of a lack of thermodynamic consistency.²⁹

Overall, the INTERFACE force field reproduces a wide spectrum of properties in quantitative agreement with measurements, including structure and unit cell geometry, surface energies, interface energies, anisotropies, and approximate mechanical properties (Table 1). Alternative force fields of inorganic compounds have typically been fitted empirically to a subset of one or two macroscopic properties, underperforming in others and in surface properties in particular. Thermodynamically consistent parametrizations, in contrast, exploit the limits of possible accuracy, and a systematic chemical understanding of force field parameters for compounds across the periodic table maximizes the predictive power.

4.2. Examples. The utility of the INTERFACE force field lies in solving experimental challenges by providing explanations and predictions about the behavior of matter. Five examples are shared here, and more information can be found in the Supporting Information (section S5).

4.2.1. Interfaces of Metallic Nanostructures. Structural information on metallic nanostructures is accessible at sub-angstrom resolution by X-ray diffraction and imaging (TEM, AFM).^{3–5} At the same time, the location of adsorbed proteins, polyelectrolytes, and surfactants in solution remains largely uncertain at nanometer resolution, and indirect information from CD, DLS, EDS, EELS, EXAFS, CD, IR, and NMR requires further interpretation. Simulation studies helped elucidate binding conformations and a soft epitaxial adsorption mechanism of peptides and surfactants on even Au and Pd surfaces, faceted nanoparticles, and other shaped metal surfaces in solution.^{51–54} Design rules for metal binding molecules were identified by simulation and explain preferences for specific facets and shapes and help us to understand the catalytic activity observed in experiment (more details in section S5.1).^{53–55}

4.2.2. Selective Adsorption onto Silica Surfaces. The composition of mineral surfaces in vacuum can be precisely examined using XPS, IR, and NMR. However, changes in the surface structure of oxides, apatites, clays, and amorphous materials in response to hydration, pH, and ionic strength cannot be easily quantified (refs 3, 7, 71–73, S16). Interactions of such nanocrystal surfaces with chain molecules control the growth rates, the shape of minerals, and are also difficult to monitor. Modeling and simulation helped to resolve surface structures and molecular assembly mechanisms. The INTERFACE force field indicates changes in the properties of silica surfaces terminated by Si–OH groups and Si–O⁻ Na⁺ groups in various ratios depending on the particle size and pH.⁷ Variations in the cation penetration depth into the aqueous phase and controlling factors for the selective binding of peptides were identified to be in agreement with zeta potential measurements, spectroscopy, and adsorption isotherms. Differences in ion pairing, hydrogen bonds, conformation effects, and binding energies for mutant peptides that differ only by a single amino acid have been computed to be in agreement with adsorption measurements.⁷

4.2.3. Self-Assembly of Surfactants on Clay Mineral Surfaces. The structure and dynamics of intercalated molecules in layered silicates play a role in the dispersion in nanocomposites, soil properties, drilling media, and cosmetics. Binding affinities and interfacial structures are difficult to track by measurement. Simulations explained the interlayer arrangement, tilt angle, conformations, and thermal transitions for an extensive series of self-assembled ammonium surfactants on mica and montmorillonites in agreement with XRD, IR, and DSC data.^{11,65,66} A predictive relationship among the packing density, tilt angles, and thermal transitions of homogeneously grafted

alkyl layers to clay mineral, metal, oxide, and halide surfaces has been derived.⁷⁵ Simulations also aided in the analysis of the cis–trans isomerization of confined azobenzene-modified surfactants in comparison to UV and XRD data,⁶⁷ the mechanism of layer cleavage of organoclays in nanocomposites to lower exfoliation energies,⁵⁰ and the analysis of nanomechanical properties of layered silicates in comparison to TEM, AFM, and Brillouin data.^{13,76} Simulations in aqueous solution explain the adsorption mechanism of peptides identified by a phage display (further details in section S5.2).⁷⁷

4.2.4. Surface Properties and Hydration of Cement Minerals. Cement is a mixture of different solid phases, including tricalcium silicate, dicalcium silicate, tricalcium aluminate, ferrite, and traces of gypsum. In the presence of water and polymeric additives, a complex combination of hydrated phases forms that contains ettringite, tobermorites, calcium hydroxide, and C–S–H.^{71,72} Interfacial processes and the action of organic additives leave many open questions. The INTERFACE force field supports a quantitative understanding of surface energies, solid–water interfacial energies, mechanical properties, and interactions of organic modifiers with all major phases and morphologies that are difficult to access by measurements.^{47,48} As an example, the performance of organic modifiers in preventing the agglomeration of tricalcium silicate particles during ball milling has been understood to be in good agreement with measurements, the anisotropy of the adsorption of polymers on various hydrated surfaces has been quantified on a molecular level, and guidance in the modification of the shape of gypsum crystals in aqueous solutions with different additives can be obtained.

4.2.5. Interfaces of Apatites with Biomolecules. Human bone and teeth are highly adaptable phosphate–organic composites.^{73,74} The characterization of interfacial processes involved in growth, decay, and related diseases remains difficult on the molecular level. Extensions of biomolecular force fields for hydroxyapatite (and fluoroapatite, in progress) allow insight into the interfaces of different degrees of hydration and dissociation, specific surface interactions, and assembly mechanisms on the nanoscale. As a first step, computed hydration energies and interactions of different cleavage planes of hydroxyapatite with peptides have shown good correlations with measured bulk hydration data, NMR, and sequence data from phage displays.⁴⁸

4.3. Limitations. General limitations of classical force fields are the exclusion of chemical reactions, the sensitivity of force field parameters to significant deviations from the reference state (temperature, pressure, and the chemical environment), and the approximate nature of combination rules.

The inability to simulate chemical reactions that involve the formation or dissociation of chemical bonds is likely the greatest limitation. Reactive systems usually require quantum-mechanical simulations using a subset of atoms or the cautious use of reactive force fields.^{34,78} For selected hydration, photoisomerization, and dissociation reactions, the INTERFACE force field suffices using minor modifications (section S5.3).^{47,67}

The sensitivity of thermodynamically consistent force field parameters to deviations from the reference state, for which they were derived, can be substantial. When derived at room temperature and standard pressure, parameters typically require no substantial re-evaluation in the temperature range of ± 200 K.⁴⁰ Necessary adjustments in parameters as a function of pressure depend on the elastic modulus of the compound. For example, higher pressures are acceptable without parameter adjustments for metals and ceramics than for liquids and gases. Significant changes in the chemical environment may also

necessitate changes in parameters. This can be the case when the aggregate state changes from liquid to gas. The dipole moment of water, for example, is significantly lower in the gas phase (O charge of $-0.66e$) than in the liquid phase (O charge lower than $-0.82e$ as a result of hydrogen bonds), which needs to be taken into account for accurate simulations of liquid–vapor equilibria.

Some dependencies of the parameters on the chemical environment can be taken into account by polarizable force fields (refs 29, 38, and S5). Polarizable models increase the number of parameters and the interpretation effort; for example, instead of a single atomic charge for each atom, core and shell charges may be coupled at a distance with a force constant and a mass for the shell charge (i.e., one parameter is expanded to five parameters). This approach can be advantageous if the base parameters are reliable (base charges, well depths, and torsion barriers; see Table 2). Because deficiencies in base parameters cannot be corrected, however, the priority of refinement would be strongly focused on base parameters first and on polarizable extensions second.

Combination rules are a smaller source of uncertainty. The use of different, justifiable combination rules leads to deviations in interfacial properties in the low percent range (Figure 2b).^{40,79} Uncertainties in interfacial properties are therefore typically below 10%. Special circumstances may suggest the use of nonstandard combination rules, for example, when there are large differences in the chemical nature and in $\epsilon_{0,ii}$ values. This could be indicated in the case of the interaction of metals with hydrocarbons (not pursued here for simplicity).

Computed elastic moduli of compounds made of smaller units that are nonbonded, such as isolated silicates, ring silicates, sulfates, and phosphates, are reproduced in very good agreement with experiment. In contrast, the assumption of rigid covalent bonding frameworks for solids in the force field that in truth share substantial ionic as well as covalent bonding contributions may lead to overestimates of computed elastic moduli while not affecting surface and interface properties. This is the case, for example, for in-plane elastic moduli of clay minerals.¹³ Differences of up to 20% in computed mechanical properties can also arise upon changes from a 9–6 LJ potential to a 12–6 LJ potential related to the difference in the repulsive properties of the potentials. The best approximation of experimental mechanical properties is sometimes achieved using a 12–6 potential (e.g., metals), sometimes using 9–6 LJ potentials, or both. A case-by-case check of a given compound using the respective reference is recommended.

5. CONCLUSIONS AND PERSPECTIVES

We described the derivation of thermodynamically consistent force field parameters for inorganic compounds to enable accurate simulations of inorganic–organic and inorganic–biomolecular interfaces using a single harmonic energy expression. The approach has been extensively tested over the past decade and applied to a range of inorganic compounds, including clay minerals, silicates, and aluminates in cement, fcc metals, sulfates, apatites, and poly(ethylene oxide). The parameters are summarized in the INTERFACE force field, which serves as a plug-in to common life science- and materials science-oriented harmonic force fields (PCFF, CHARMM, AMBER, COMPASS, GROMACS, and OPLS-AA).

A key aspect in thermodynamically consistent parametrization is the quantitative comparison of individual force field parameters to atomic-level measurements and the comparison of key computed bulk and surface properties to corresponding laboratory data. In particular, attention to the all-inclusive understanding of sensitive atomic charges and van der Waals

parameters in the context of available physical–chemical data and theory was found to be detrimental. The new parametrization enables an array of properties to agree quantitatively with measurements. These include the density, dipole moment, cleavage energy, surface tension, hydration energy (for stable, nonreactive surfaces), solid–liquid interfacial tension, anisotropies of surface properties for individual $\{hkl\}$ facets, and adsorption energies of organic and biomolecular compounds. Moreover, computed dielectric, thermal, and elastic properties agree well with experiment. The accuracy is comparable to that of QM simulations and outperforms that of specialized force fields.

The described approach resolves discrepancies between computed and measured surface properties of up to 2 orders of magnitude in alternative force fields for inorganic compounds and eases the transferability of intermolecular potentials. Alternative methods often fail because of automated nonbonding parametrizations that involve unverified assumptions, discrepancies with available laboratory data, and empirical parameter fitting to match selected properties while accepting large deviations in others. The present approach largely eliminates uncertainties by providing an understanding of parameters, facilitates the use of uniform force fields for a wide range of materials (e.g., including biopolymers, metals, and minerals), and exploits the limits of force field performance.

Thermodynamic consistency also provides fertile ground for force field extensions beyond traditional performance, including polarizability, temperature-dependent and pressure-dependent parameters for behavior under extreme conditions, chemically better justified potentials for reactions, and models in adaptive resolution for multiscale simulations. The INTERFACE force field can help solve problems in materials and life sciences, for example, molecular recognition at metal and mineral surfaces, growth and shape control of inorganic–organic nanostructures, and self-organization in solution.

■ ASSOCIATED CONTENT

Supporting Information

The INTERFACE-PCFF force field, including force field parameters, atomistic models, and documentation. Additional information for the main text: (1) an overview of multiscale simulation methods, (2) recent trends in interface simulations, (3) the role of combination rules for thermodynamic consistency, (4) derivation of force field parameters in detail, including existing sources and new developments, atomic charges, van der Waals parameters, bonding parameters, interfaces and multiphase materials, available versions of the INTERFACE force field and adaptation to other force field expressions, parametrization of new compounds, (5) further validation and possible extensions, including the reliability of LJ parameters for fcc metals, layered silicates, comparison with reactive potentials and other potential types, (6) a one-page overview of the INTERFACE force field, and (7) additional references. This material is available free of charge via the Internet at <http://pubs.acs.org>.

■ AUTHOR INFORMATION

Corresponding Author

*E-mail: hendrik.heinz@uakron.edu.

Notes

The authors declare no competing financial interest.

■ ACKNOWLEDGMENTS

We acknowledge support from the National Science Foundation (DMR-0955071), the Air Force Research Laboratory, UES, Inc., Sika AG, the Procter & Gamble Company, the University of Akron, and the Ohio Supercomputing Center for the allocation of computational resources. We are grateful for discussions with William A. Goddard III (California Institute of Technology), Robert J. Flatt (ETH Zurich), Ras B. Pandey (University of Southern Mississippi), Rajiv J. Berry, Barry L. Farmer, Gary Kedziora, and Rajesh R. Naik (Wright-Patterson AFB), and Jie Feng, Kshitij C. Jha, Hadi Ramezani-Dakhel, and Hua Liu (University of Akron).

■ REFERENCES

- (1) Peer, D.; Karp, J. M.; Hong, S.; Farokhzad, O. C.; Margalit, R.; Langer, R. Nanocarriers: Emerging Platforms for Cancer Therapy. *Nat. Nanotechnol.* **2007**, *2*, 751–760.
- (2) Bita, I.; Yang, J. K. W.; Jung, Y. S.; Ross, C. A.; Thomas, E. L.; Berggren, K. K. Graphoepitaxy of Self-Assembled Block Copolymers on Two-Dimensional Periodic Patterned Templates. *Science* **2008**, *321*, 939–943.
- (3) Dickerson, M. B.; Sandhage, K. H.; Naik, R. R. The Protein and Peptide-Directed Syntheses of Inorganic Materials. *Chem. Rev.* **2008**, *108*, 4935–4978.
- (4) Coppage, R.; Slocik, J. M.; Sethi, M.; Pacardo, D. B.; Naik, R. R.; Knecht, M. R. Elucidation of Peptide Effects That Control the Activity of Nanoparticles. *Angew. Chem., Int. Ed.* **2010**, *49*, 3767–3770.
- (5) Chiu, C.-Y.; Li, Y.; Ruan, L.; Ye, X.; Murray, C. B.; Huang, Y. Platinum Nanocrystals Selectively Shaped Using Facet-Specific Peptide Sequences. *Nat. Chem.* **2011**, *3*, 393–399.
- (6) Feng, J.; Cavicchi, K. A.; Heinz, H. Control over Self-Assembly of Diblock Copolymers on Hexagonal and Square Templates for High Area Density Circuit Boards. *ACS Nano* **2011**, *5*, 9413–9420.
- (7) Patwardhan, S. V.; Emani, F. S.; Berry, R. J.; Jones, S. E.; Naik, R. R.; Deschaume, O.; Heinz, H.; Perry, C. C. Chemistry of Aqueous Silica Nanoparticle Surfaces and the Mechanism of Selective Peptide Adsorption. *J. Am. Chem. Soc.* **2012**, *134*, 6244–6256.
- (8) Frenkel, D.; Smit, B. *Understanding Molecular Simulation*; Academic Press: San Diego, 2002.
- (9) Praprotnik, M.; Delle Site, L.; Kremer, K. Multiscale Simulation of Soft Matter: From Scale Bridging to Adaptive Resolution. *Annu. Rev. Phys. Chem.* **2008**, *59*, 545–571.
- (10) Zhao, Y.; Truhlar, D. G. Density Functionals with Broad Applicability in Chemistry. *Acc. Chem. Res.* **2008**, *41*, 157–167.
- (11) Heinz, H.; Castelijns, H. J.; Suter, U. W. Structure and Phase Transitions of Alkyl Chains on Mica. *J. Am. Chem. Soc.* **2003**, *125*, 9500–9510.
- (12) Benitez, D.; Shapiro, N. D.; Tkatchouk, E.; Wang, Y. M.; Goddard, W. A.; Toste, F. D. A Bonding Model for Gold(I) Carbene Complexes. *Nat. Chem.* **2009**, *1*, 482–486.
- (13) Zartman, G. D.; Liu, H.; Akdim, B.; Pachter, R.; Heinz, H. Nanoscale Tensile, Shear, and Failure Properties of Layered Silicates as a Function of Cation Density and Stress. *J. Phys. Chem. C* **2010**, *114*, 1763–1772.
- (14) Heinz, H.; Koerner, H.; Vaia, R. A.; Anderson, K. L.; Farmer, B. L. Force Field for Phyllosilicates and Dynamics of Octadecylammonium Chains Grafted to Montmorillonite. *Chem. Mater.* **2005**, *17*, 5658–5669.
- (15) Born, M. Eine Thermochemische Anwendung der Gittertheorie. *Verh. Dtsch. Phys. Ges.* **1919**, *21*, 13–24.
- (16) Jones, J. E. On the Determination of Molecular Fields. II. From the Equation of State of a Gas. *Proc. R. Soc. London, Ser. A* **1924**, *106*, 463–477.
- (17) Jones, J. E.; Ingham, A. E. On the Calculation of Certain Crystal Potential Constants, and on the Cubic Crystal of Least Potential Energy. *Proc. R. Soc. London, Ser. A* **1925**, *107*, 636–653.

- (18) Pearlman, D. A.; Case, D. A.; Caldwell, J. W.; Ross, W. S.; Cheatham, T. E.; DeBolt, S.; Ferguson, D.; Seibel, G.; Kollman, P. AMBER, a Package of Computer Programs for Applying Molecular Mechanics, Normal Mode Analysis, Molecular Dynamics and Free Energy Calculations to Simulate the Structural and Energetic Properties of Molecules. *Comput. Phys. Commun.* **1995**, *91*, 1–41.
- (19) MacKerell, A. D., Jr.; Bashford, D.; Bellott, R. L.; Dunbrack, R. L., Jr.; Evanseck, J. D.; Field, M. J.; Fischer, S.; Gao, J.; Guo, H.; Ha, S.; Joseph-McCarthy, D.; Kuchnir, L.; Kuczera, K.; Lau, F. T. K.; Mattos, C.; Michnick, S.; Ngo, T.; Nguyen, D. T.; Prodhom, B.; Reiher, W. E., III; Roux, B.; Schlenkrich, M.; Smith, J. C.; Stote, R.; Straub, J.; Watanabe, M.; Wiorkiewicz-Kuczera, J.; Yin, D.; Karplus, M. All-Atom Empirical Potential for Molecular Modeling and Dynamics Studies of Proteins. *J. Phys. Chem. B* **1998**, *102*, 3586–3616.
- (20) Sun, H. COMPASS: An Ab Initio Force-Field Optimized for Condensed-Phase Applications – Overview with Details on Alkane and Benzene Compounds. *J. Phys. Chem. B* **1998**, *102*, 7338–7364.
- (21) Dauber-Osguthorpe, P.; Roberts, V. A.; Osguthorpe, D. J.; Wolff, J.; Genest, M.; Hagler, A. T. Structure and Energetics of Ligand Binding to Proteins: Escherichia Coli Dihydrofolate Reductase-Trimethoprim, a Drug-Receptor System. *Proteins: Struct., Funct., Genet.* **1988**, *4*, 31–47.
- (22) Mayo, S. L.; Olafson, B. D.; Goddard, W. A. DREIDING: A Generic Force Field for Molecular Simulations. *J. Phys. Chem.* **1990**, *94*, 8897–8909.
- (23) Berendsen, H. J. C.; van der Spoel, D.; van Drunen, R. GROMACS: A Message-Passing Parallel Molecular Dynamics Implementation. *Comput. Phys. Commun.* **1995**, *91*, 43–56.
- (24) Hess, B.; Kutzner, C.; van der Spoel, D.; Lindahl, E. GROMACS 4: Algorithms for Highly Efficient, Load-Balanced, and Scalable Molecular Simulation. *J. Chem. Theory Comput.* **2008**, *4*, 435–447.
- (25) Halgren, T. A. Merck Molecular Force Field. I. Basis, Form, Scope, Parameterization, and Performance of MMFF94. *J. Comput. Chem.* **1996**, *17*, 490–519.
- (26) Jorgensen, W. L.; Maxwell, D. S.; Tirado-Rives, J. Development and Testing of the OPLS All-Atom Force Field on Conformational Energetics and Properties of Organic Liquids. *J. Am. Chem. Soc.* **1996**, *118*, 11225–11236.
- (27) A series of references beginning with Sun, H.; Mumby, S. J.; Maple, J. R.; Hagler, A. T. An Ab-Initio CFF93 All-Atom Force Field for Polycarbonates. *J. Am. Chem. Soc.* **1994**, *116*, 2978–2987. The complete list is given in ref S1 in the Supporting Information.
- (28) Rai, N.; Siepmann, J. I. Transferable Potentials for Phase Equilibria. 9. Explicit Hydrogen Description of Benzene and Five-Membered and Six-Membered Heterocyclic Aromatic Compounds. *J. Phys. Chem. B* **2007**, *111*, 10790–10799.
- (29) Fang, C. M.; Parker, S. C.; de With, G. Atomistic Simulation of the Surface Energy of Spinel $MgAl_2O_4$. *J. Am. Ceram. Soc.* **2000**, *83*, 2082–2084. In addition, see also refs S2 and S3 in the Supporting Information.
- (30) Spagnoli, D.; Cooke, D. J.; Kerisit, S.; Parker, S. C. Molecular Dynamics Simulations of the Interaction Between the Surfaces of Polar Solids and Aqueous Solutions. *J. Mater. Chem.* **2006**, *16*, 1997–2006.
- (31) Park, S. H.; Sposito, G. Structure of Water Adsorbed on a Mica Surface. *Phys. Rev. Lett.* **2002**, *89*, 085501.
- (32) Smith, G. D.; Borodin, O.; Bedrov, D. A Revised Quantum Chemistry-Based Potential for Poly(ethylene oxide) and its Oligomers in Aqueous Solution. *J. Comput. Chem.* **2002**, *23*, 1480–1488.
- (33) Daw, M. S.; Foiles, S. M.; Baskes, M. I. The Embedded-Atom Method: A Review of Theory and Applications. *Mater. Sci. Rep.* **1992**, *9*, 251–310.
- (34) Chenoweth, K.; van Duin, A. C. T.; Goddard, W. A. ReaxFF Reactive Force Field for Molecular Dynamics Simulations of Hydrocarbon Oxidation. *J. Phys. Chem. A* **2008**, *112*, 1040–1053.
- (35) Tersoff, J. Empirical Interatomic Potential for Carbon, with Application to Amorphous Carbon. *Phys. Rev. Lett.* **1988**, *61*, 2879–2882.
- (36) Brenner, D. W. Empirical Potential for Hydrocarbons for Use in Simulating the Chemical Vapor Deposition of Diamond Films. *Phys. Rev. B* **1990**, *42*, 9458–9471.
- (37) Stuart, S. J.; Tutein, A. B.; Harrison, J. A. A Reactive Potential for Hydrocarbons with Intermolecular Interactions. *J. Chem. Phys.* **2000**, *112*, 6472–6486.
- (38) Ponder, J. W.; Wu, C. J.; Ren, P. Y.; Pande, V. S.; Chodera, J. D.; Schnieders, M. J.; Haque, I.; Mobley, D. L.; Lambrecht, D. S.; DiStasio, R. A.; Head-Gordon, M.; Clark, G. N. I.; Johnson, M. E.; Head-Gordon, T. Current Status of the AMOEBA Polarizable Force Field. *J. Phys. Chem. B* **2010**, *114*, 2549–2564.
- (39) See refs S4–S13 in the Supporting Information.
- (40) Heinz, H.; Vaia, R. A.; Farmer, B. L.; Naik, R. R. Accurate Simulation of Surfaces and Interfaces of FCC Metals Using 12–6 and 9–6 Lennard-Jones Potentials. *J. Phys. Chem. C* **2008**, *112*, 17281–17290.
- (41) Segvich, S.; Biswas, S.; Becker, U.; Kohn, D. H. Identification of Peptides with Targeted Adhesion to Bone-Like Mineral via Phage Display and Computational Modeling. *Cells Tissues Organs* **2009**, *189*, 245–251.
- (42) Iori, F.; Di Felice, R.; Molinari, E.; Corni, S. GolP: An Atomistic Force-Field to Describe the Interaction of Proteins with Au(111) Surfaces in Water. *J. Comput. Chem.* **2009**, *30*, 1465–1476.
- (43) Pellenq, R. J.-M.; Kushima, A.; Shahsavari, R.; Van Vliet, K. J.; Buehler, M. J.; Yip, S.; Ulm, F.-J. A Realistic Molecular Model of Cement Hydrates. *Proc. Natl. Acad. Sci. U.S.A.* **2009**, *106*, 16102–16107.
- (44) Oren, E. E.; Notman, R.; Kim, I. W.; Evans, J. S.; Walsh, T. R.; Samudrala, R.; Tamerler, C.; Sarikaya, M. Probing the Molecular Mechanisms of Quartz-Binding Peptides. *Langmuir* **2010**, *26*, 11003–11009.
- (45) Monti, S.; Walsh, T. R. Molecular Dynamics Simulations of the Adsorption and Dynamical Behavior of Single DNA Components on TiO_2 . *J. Phys. Chem. C* **2011**, *115*, 24238–24246.
- (46) Butenuth, A.; Moras, G.; Schneider, J.; Koleini, M.; Koppen, S.; Meissner, R.; Wright, L. B.; Walsh, T. R.; Ciacchi, L. C. Ab-Initio Derived Force-Field Parameters for Molecular Dynamics Simulations of Deprotonated Amorphous-SiO₂/Water Interfaces. *Phys. Status Solidi B* **2012**, *249*, 292–305.
- (47) Mishra, R. K. *Simulation of Interfaces in Construction Materials: Tricalcium Silicate, Gypsum, and Organic Modifiers*. Ph.D. Dissertation, University of Akron, 2012.
- (48) Work reported here and in progress.
- (49) Heinz, H.; Vaia, R. A.; Farmer, B. L. Interaction Energy and Surface Reconstruction between Sheets of Layered Silicates. *J. Chem. Phys.* **2006**, *124*, 224713.
- (50) Fu, Y. T.; Heinz, H. Structure and Cleavage Energy of Surfactant-Modified Clay Minerals: Influence of CEC, Head Group, and Chain Length. *Chem. Mater.* **2010**, *22*, 1595–1605.
- (51) Heinz, H.; Jha, K. C.; Luettmer-Strathmann, J.; Farmer, B. L.; Naik, R. R. Polarization at Metal-Biomolecular Interfaces in Solution. *J. R. Soc., Interface* **2011**, *8*, 220–232.
- (52) Heinz, H.; Farmer, B. L.; Pandey, R. B.; Slocik, J. M.; Patnaik, S. S.; Pachter, R.; Naik, R. R. Nature of Molecular Interactions of Peptides with Gold, Palladium, and Pd-Au Bimetal Surfaces in Aqueous Solution. *J. Am. Chem. Soc.* **2009**, *131*, 9704–9714.
- (53) Feng, J.; Pandey, R. B.; Berry, R. J.; Farmer, B. L.; Naik, R. R.; Heinz, H. Adsorption Mechanism of Single Amino Acid and Surfactant Molecules to Au {111} Surfaces in Aqueous Solution: Design Rules for Metal-Binding Molecules. *Soft Matter* **2011**, *7*, 2113–2120.
- (54) Feng, J.; Slocik, J. M.; Sarikaya, M.; Naik, R. R.; Farmer, B. L.; Heinz, H. Influence of the Shape of Nanostructured Metal Surfaces on Adsorption of Single Peptide Molecules in Aqueous Solution. *Small* **2012**, *8*, 1049–1059.
- (55) Coppage, R.; Slocik, J. M.; Briggs, B. D.; Frenkel, A. I.; Heinz, H.; Naik, R. R.; Knecht, M. R. Crystallographic Recognition Controls Peptide Binding for Bio-Based Nanomaterials. *J. Am. Chem. Soc.* **2011**, *133*, 12346–12349.
- (56) Additional terms of higher order in class II force fields originate by analogy to perturbation theory in quantum mechanics and increase the burden of parametrization. The physical justification for these terms is debatable so that class II force fields can be treated as class I force fields for new developments. The remaining class II terms for existing

compounds have no adverse effect and maintain the consistency of the parameters.

(57) A temperature of zero Kelvin for surface atoms can accelerate the initial equilibration; however, the quantitative analysis of interfacial properties requires the thermal motion of all atoms consistent with experimental conditions (temperature and pressure).

(58) Heinz, H.; Suter, U. W. Atomic Charges for Classical Simulations of Polar Systems. *J. Phys. Chem. B* **2004**, *108*, 18341–18352.

(59) Giese, R. F.; van Oss, C. J. *Colloid and Surface Properties of Clays and Related Minerals*; Marcel Dekker: New York, 2002.

(60) CRC Handbook of Chemistry and Physics, 89th ed.; Lide, D. R., Ed.; CRC Press: Boca Raton, FL, 2008.

(61) Batsanov, S. S. van der Waals Radii of Elements. *Inorg. Mater.* **2001**, *37*, 871–885.

(62) Hirshfeld, F. L. Bonded Atom Fragments for Describing Molecular Charge Densities. *Theor. Chim. Acta* **1977**, *44*, 129–138.

(63) Gross, K. C.; Seybold, P. G.; Hadad, C. M. Comparison of Different Atomic Charge Schemes for Predicting pK_a Variations in Substituted Anilines and Phenols. *Int. J. Quantum Chem.* **2002**, *90*, 445–458.

(64) Halgren, T. A. The Representation of van der Waals (vdW) Interactions in Molecular Mechanics Force Fields: Potential Form, Combination Rules, and vdW Parameters. *J. Am. Chem. Soc.* **1992**, *114*, 7827–7843.

(65) Heinz, H.; Suter, U. W. Surface Structure of Organoclays. *Angew. Chem., Int. Ed.* **2004**, *43*, 2239–2243.

(66) Heinz, H.; Vaia, R. A.; Krishnamoorti, R.; Farmer, B. L. Self-Assembly of Alkylammonium Chains on Montmorillonite: Effect of Chain Length, Head Group Structure, and Cation Exchange Capacity. *Chem. Mater.* **2007**, *19*, 59–68.

(67) Heinz, H.; Vaia, R. A.; Koerner, H.; Farmer, B. L. Photoisomerization of Azobenzene Grafted to Layered Silicates: Simulation and Experimental Challenges. *Chem. Mater.* **2008**, *20*, 6444–6456.

(68) Mehl, M. J.; Papaconstantopoulos, D. A. Applications of a Tight-Binding Total-Energy Method for Transition and Noble Metals: Elastic Constants, Vacancies, and Surfaces of Monatomic Metals. *Phys. Rev. B* **1996**, *54*, 4519–4530.

(69) Jarvi, T. T.; Kuronen, A.; Hakala, M.; Nordlund, K.; van Duin, A. C. T.; Goddard, W. A.; Jacob, T. Development of a ReaxFF Description for Gold. *Eur. Phys. J. B* **2008**, *66*, 75–79.

(70) Keith, J. A.; Fantauzzi, D.; Jacob, T.; van Duin, A. C. T. Reactive Forcefield for Simulating Gold Surfaces and Nanoparticles. *Phys. Rev. B* **2010**, *81*, 235404.

(71) Bullard, J. W. A Determination of Hydration Mechanisms for Tricalcium Silicate Using a Kinetic Cellular Automaton Model. *J. Am. Ceram. Soc.* **2008**, *91*, 2088–2097.

(72) Juillard, P.; Gallucci, E.; Flatt, R.; Scrivener, K. Dissolution Theory Applied to the Induction Period in Alite Hydration. *Cem. Concr. Res.* **2010**, *40*, 831–844.

(73) Kirkham, J.; Brookes, S. J.; Shore, R. C.; Wood, S. R.; Smith, D. A.; Zhang, J.; Chen, H.; Robinson, C. Physico-Chemical Properties of Crystal Surfaces in Matrix–Mineral Interactions during Mammalian Biominerallisation. *Curr. Opin. Colloid Interface Sci.* **2002**, *7*, 124–132.

(74) Weiger, M. C.; Park, J. J.; Roy, M. D.; Stafford, C. M.; Karim, A.; Becker, M. L. Quantification of the Binding Affinity of a Specific Hydroxyapatite Binding Peptide. *Biomaterials* **2010**, *31*, 2955–2963.

(75) Heinz, H.; Vaia, R. A.; Farmer, B. L. Relation between Packing Density and Thermal Transitions of Alkyl Chains on Layered Silicate and Metal Surfaces. *Langmuir* **2008**, *24*, 3727–3733.

(76) Fu, Y. T.; Zartman, G. D.; Yoonessi, M.; Drummy, L. F.; Heinz, H. Bending of Layered Silicates on the Nanometer Scale: Mechanism, Stored Energy, and Curvature Limits. *J. Phys. Chem. C* **2011**, *115*, 22292–22300.

(77) Heinz, H. Clay Minerals for Nanocomposites and Biotechnology: Surface Modification, Dynamics, and Responses to Stimuli. *Clay Miner.* **2012**, *47*, 205–230.

(78) Varshney, V.; Patnaik, S. S.; Roy, A. K.; Farmer, B. L. A Molecular Dynamics Study of Epoxy-Based Networks: Cross-linking Procedure

and Prediction of Molecular and Material Properties. *Macromolecules* **2008**, *41*, 6837–6842.

(79) Delhommele, J.; Millie, P. Inadequacy of the Lorentz-Berthelot Combining Rules for Accurate Predictions of Equilibrium Properties by Molecular Simulation. *Mol. Phys.* **2001**, *99*, 619–625.

Supporting Information

Thermodynamically Consistent Force Fields for the Assembly of Inorganic, Organic, and
Biological Nanostructures: The INTERFACE Force Field

By

Hendrik Heinz, Tzu-Jen Lin, Ratan Kishore Mishra, Fateme Sadat Emami

Department of Polymer Engineering, University of Akron, Akron, OH 44325

Email: hendrik.heinz@uakron.edu

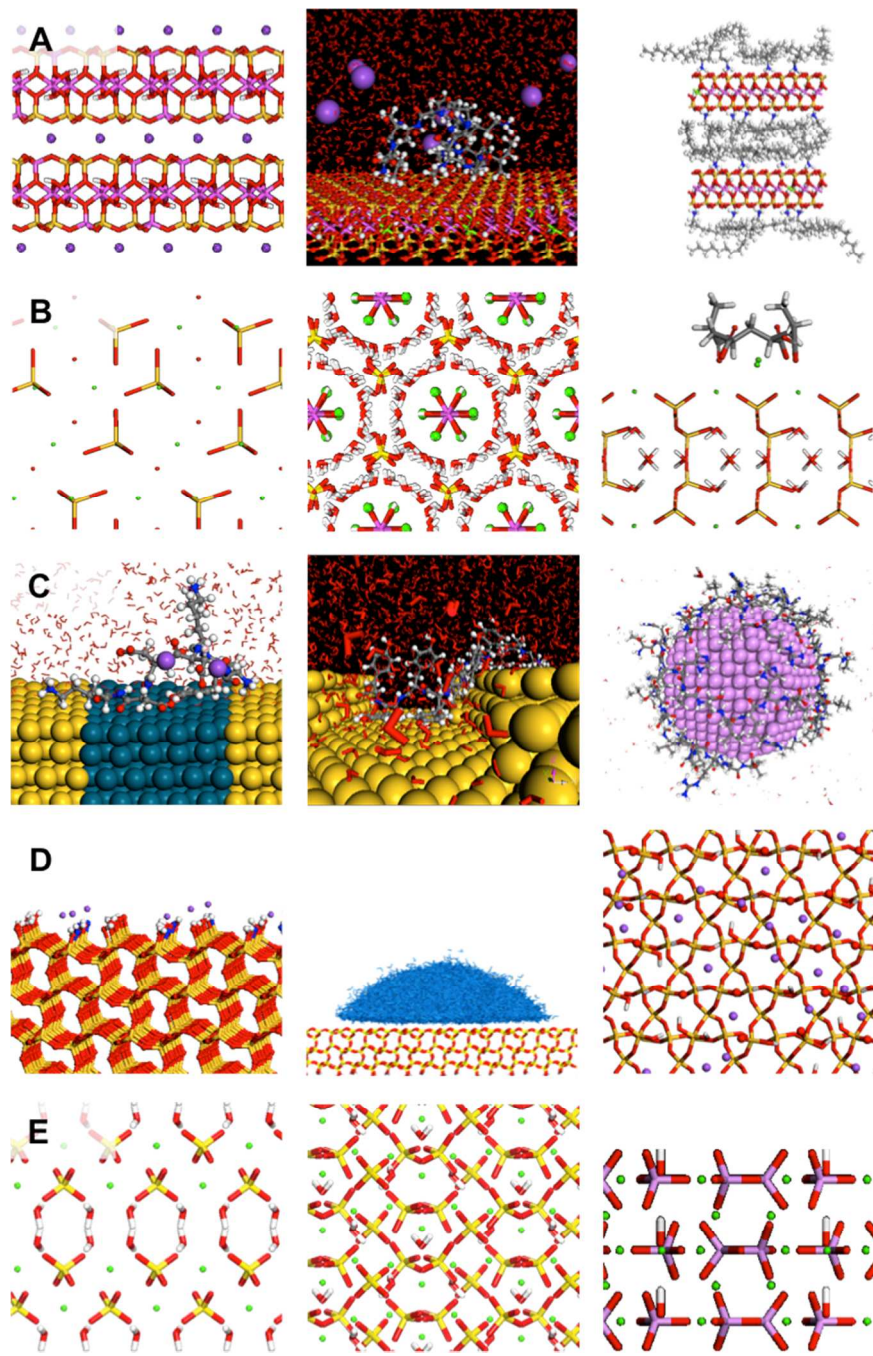


Figure S1. Examples of structures and interfaces simulated using the INTERFACE force field (left to right in each row). (A) Layered silicates, including mica, montmorillonite in contact with a peptide in aqueous solution, and montmorillonite modified with alkylammonium surfactants. (B) Cement minerals, depicting tricalcium silicate, ettringite, and tobermorite 11 Å in contact with an organic additive. (C) Fcc metals with the examples of a gold-palladium bimetal surface, a stepped gold surface, and a platinum nanoparticle in contact with peptides in aqueous solution. (D) An ionized Q³ silica surface, water in contact with a Q⁴ silica surface, and top view onto an ionized Q² silica surface. (E) Impressions of the crystal structures of gypsum, calcium sulphate hemihydrate, and hydroxyapatite.

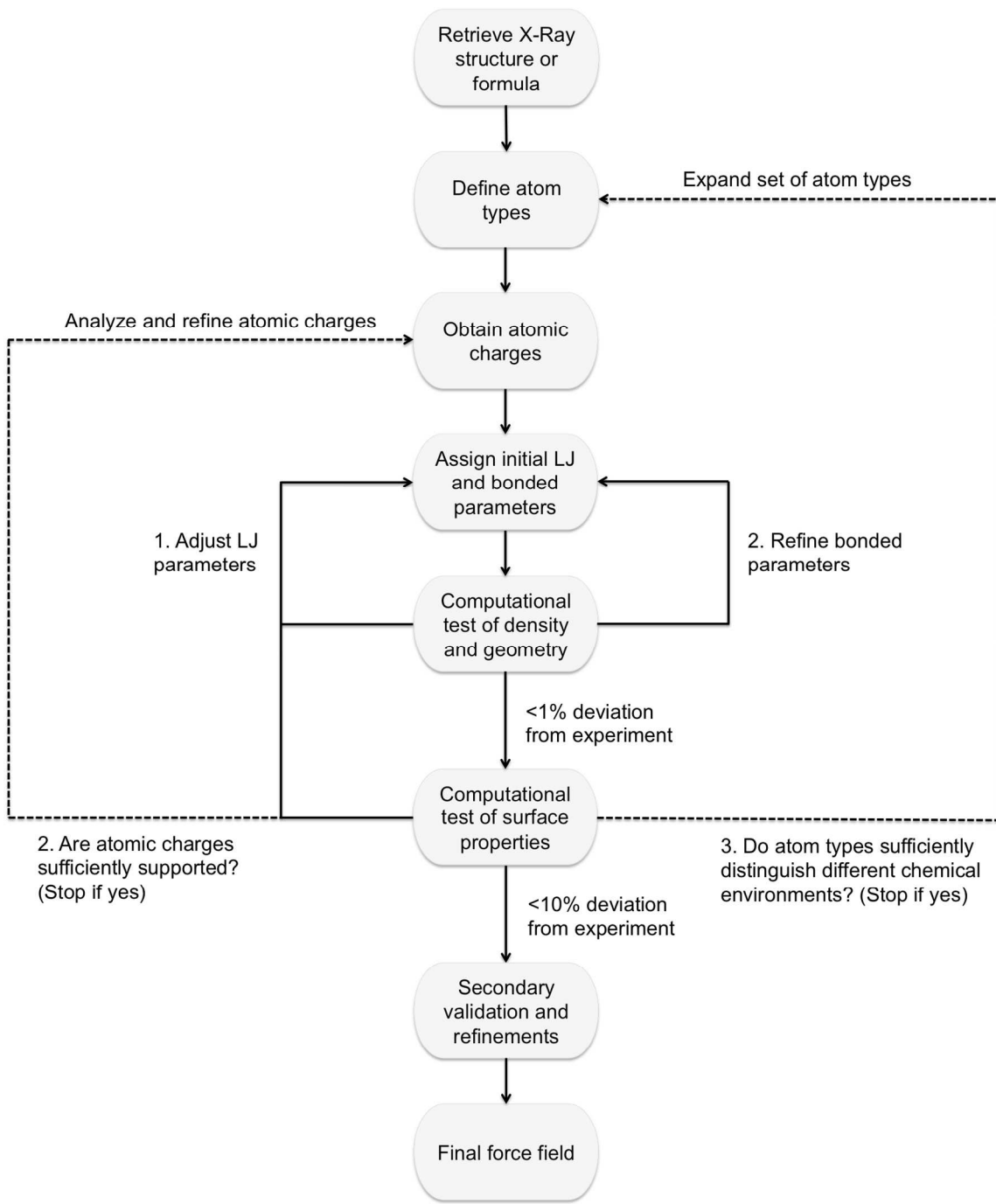


Figure S2. Procedure for parameterization of new and existing compounds in the INTERFACE force field, including the most common refinement loops. Careful assignments in every step in full agreement with physical and chemical understanding minimize the need for loops. In principle, it is possible to go back to any prior step at each stage in the procedure until thermodynamic consistency is achieved. See text in sections 3 and S4.

Table S1. Atomic charges for selected compounds from experimentally measured electron deformation densities and partition into spherical atomic basins using the Hirshfeld method. The values provide a valuable starting point for molecular simulations, especially for polar compounds containing heavy elements. Standard deviations of the last digit are given in brackets (extension of an earlier compilation in ref. 58).

Compound	Atom	Charge in units of e	Reference
LiF	Li	0.95 (3)	S19b
LiI	Li	0.67 (5)	S22b
LiNO ₂ · H ₂ O	Li(H ₂ O)	0.83	S22a
	N	0.51	
	O (nitrite)	-0.67	
NaCl	Na	1.00 (0)	S19b
NaNO ₃ ^a	Na	0.95 (5)	S20b
	N	-0.20 (10)	
	O	-0.25 (10)	
KBr	K	0.8 (1)	S19c
CaF ₂	Ca	2.00 (0)	S19b
MgO	Mg	1.6 (2)	S19a
Al ₂ O ₃	Al	1.32 (5)	S21
AlO(OH)	Al	1.47 (27)	S19d
	H	0.20 (5)	
AlPO ₄ ^b	Al	1.4 (1)	S20a
	P	1.0 (1)	
CrSO ₄ · 5 H ₂ O ^c	Cr(H ₂ O) ₅	0.96 (20)	S23
	S	0.24 (6)	
	O (sulfate)	-0.30 (6)	
Co[O(NC ₅ H ₅) ₆ (ClO ₄) ₂	Co	1.74 (4)	S24
	Cl	-0.12 (1)	
	O (perchlorate)	-0.15 (4)	
	Pyridine-N-oxide ligand	-0.05 (5) [individual: O -0.83, N 0.27, C ~ -0.2, H ~ 0.3]	
CuSO ₄ · 5 H ₂ O ^c	Cu(H ₂ O) ₅	1.18 (10)	S23
	S	0.06 (2)	
	O (sulphate)	-0.31 (6)	
Cu ₆ Si ₆ O ₁₈ · 6 H ₂ O	Cu	1.23 (6)	S25
	Si	1.17 (15)	
	O (water)	-0.74 (6)	

^a The density of valence electrons near the middle of the N–O bond is high, leading to an uncertainty in atomic charges up to $\pm 0.1\text{e}$. ^b The crystal structure of AlPO₄ is the same as for tetrahedral SiO₂ (α -quartz) as Al and P are left and right neighbors to Si in the periodic table. The investigation was performed to obtain more information on the charge distribution in the isoelectronic SiO₂, which is noncentrosymmetric, and a Si charge of ~ 1.2 was inferred. ^c The atomic charges are averaged over different environments. Significant anisotropy was observed, such as charge transfer between the metal cation and coordinated water.

S1. An Overview of Multiscale Simulation Methods

Quantum mechanical methods enable the analysis of the geometry of molecules, conformers, and clusters of molecules including orbitals, transition states, and chemical reactions. The Schrodinger equation only provides an exact solution for one hydrogen atom while larger systems require numerical approximations.^{S27-S29} Computationally affordable and sufficiently realistic solutions of the Schrodinger equation for many electron systems remain an intense area of research.^{10,S30-S33} The best approximation of the electronic structure is obtained using full configuration interaction, which leads to a scaling of computation time with the number of electrons N as $O(N^7)$. Computations beyond small molecules, radicals, and ions are difficult due to the high exponential dependence on system size. Coupled cluster and density functional theory (DFT) methods involve approximations of basis functions, basis sets, and density functionals to reduce the compute expense from $O(N^7)$ to $O(N^3)$ and can be employed to simulate systems up to thousands of atoms. The completion of one picosecond ab-initio MD^{S30} of a peptide in 500 molecules of water using the GGA-PBE functional currently requires approximately 256 processor cores for one week. The convergence in energies using different density functionals, e.g., within the M0x classes, is often not satisfactory.^{10,S31,S34} For example, computed dissociation energies of small molecules from surfaces, cohesive energies of small organic molecules, and electronic excitation energies may differ by a factor up to two. Nevertheless, QM methods are paramount to investigate chemical reactivity and electronic properties at the local scale of chemical bonds, including electron densities, energy levels, conduction, and magnetism. QM methods are less suited to examine properties of systems containing more than several hundred atoms, and limited to time scales of picoseconds. Higher and more compute-expensive

levels of theory are required in particular when heavier elements with d and f electrons are involved.

Access to larger systems is possible using molecular dynamics and Monte Carlo simulations on the basis of a classical Hamiltonian. Compute time scales as $O(M \ln N)$ or $O(N^2)$ with the number of atoms N , depending on the type of summation of pairwise interactions. Folding and self organization of chain molecules in solution and at surfaces in all-atom resolution can be studied as a function of concentration, pH, and ionic strength.^{7,54} Longest recorded simulation times to date exceed milliseconds^{S35} and the completion of 100 nanoseconds classical MD of a protein in 1000 molecules of water with high accuracy of Coulomb interactions currently requires approximately eight processor cores for one week. Access to significant time scales and parallel simulations enables the exploration of complex configuration spaces at length scales of 1 to 1000 nm. Therefore, interfacial assembly, thermal transitions, diffusion, optical switching, and time-dependent mechanical properties can be investigated.^{7,11,51,52,54,65-67,S35,S36} A major limitation is, however, the difficulty to simulate bond dissociation and formation during chemical reactions.

The analysis of structure and dynamics at scales of 10 nm to 1000 μm and nanoseconds to seconds can be achieved using MD and MC simulations on the basis of coarse-grain models. These models involve fewer degrees of freedom compared to atomistic models as every bead represents several, tens, or hundreds of atoms according to the desired level of coarse-graining.^{S37-S39} The energy expression is also simplified, for example, it may contain only bond stretch and van-der-Waals terms.^{S40,S41} When the energy expression and molecular models are chosen interchangeably with a full atomistic description, mapping between full atomistic resolution and coarse grain resolution is possible as well as simulations in dual atomistic/coarse grain resolution. Dissipative Particle Dynamics with soft, interpenetrable particles,^{S42} and field-

based approaches^{S43} can also be employed to access similarly larger length and time scales as with coarse-grain models.

S2. Recent Trends in Interface Simulations

Recent work by many research groups illustrates the variety of problems that can be addressed using simulation techniques at different time and length scales. Current strengths and weaknesses are illustrated by representative examples in this section.

Truhlar et al. have developed state-of-the art density functionals¹⁰ and utilized the parameters to understand the adsorption of CO and NO molecules on defective MgO {100} and NiO {100} surfaces.^{S31} Chemical bonds to the surfaces can be well characterized yet computed dissociation energies vary by multiples in comparison to experiment. Electronic excitation energies of small molecules have been computed using various density functionals in very good agreement (~10%) with results from higher level methods (MS-CASPT2).^{S32} Ab-initio studies by Goddard et al on gold-carbene complexes explain possible catalytic pathways to form C–C bonds.¹² Knecht and Heinz et al have examined possible catalytic mechanisms of carbon-carbon coupling reactions on peptide-capped Pd nanocrystals using experiment and simulation.^{S55} Kremer and Mullen et al. investigated the structure and charge mobility of coronene-type stacked organic semiconductors, using QM methods to derive transfer integrals in combination with measurements.^{S44} van Duin and Goddard et al developed the Reaxx force field to describe chemical reactions of hydrocarbons, silicates, and other compounds.³⁴ Complex bond order terms and highly customized functional terms, however, make it difficult to combine parameters with existing force fields for biopolymers and organic compounds, and reproducible extensions to other compounds are extremely challenging. Ponder et al have developed polarizable force fields for

water and biomolecules (AMOEBA), aiming at better representation of polarity and conformations than all-atom force fields using extensive quantum-mechanical evaluation.³⁸ The energy expression of AMOEBA differs from harmonic force fields such as PCFF, COMPASS, AMBER, CHARMM, GROMACS, and OPLS-AA.

Parker et al calculated the surface energy of spinel using a dedicated Buckingham potential and found an overestimate by more than 50% in comparison to experiment.²⁹ Simulations of hematite and calcite in contact with water showed layering and ion dissolution effects.³⁰ Heinz et al developed a force field for mica-type silicates using common harmonic energy expressions and demonstrated quantitative agreement of computed and measured surface properties.^{11,14} The effectiveness of the approach was later utilized to derive equally dependable parameters for other inorganic compounds that are summarized in the INTERFACE force field.^{7,40,47,48} Self assembly mechanisms of surfactants, thermal transitions, and thermodynamic models for exfoliation in composites have been explained in agreement with available laboratory observations.^{11,49,50,65-67} Cygan et al developed a broader force field for clay minerals which is less accurate in surface properties.^{S10} Cygan and Kirkpatrick et al inspected the mica-water interfacial structure using classical molecular dynamics simulation in good agreement with X-Ray reflectivity data.^{S11} Walsh et al have carried out simulations of DNA binding to titania and peptides binding to quartz surfaces in aqueous solution using classical force fields, aiming at the prediction of the binding mechanism and tailored sequences in comparison to experimental data from phage display.^{45,46} The protonation state of the surfaces, however, was often disregarded. Patwardhan, Heinz, and Perry et al. quantified silica surface compositions in aqueous solution and peptide adsorption mechanisms in agreement with measurements using a thoroughly validated silica force field.⁷ Machesky et al investigated the surface protonation of titania and cassiterite (tin dioxide) using

simulation and experiment,^{S45} and Cummings et al. the adsorption of nucleotides on fullerenes.^{S46}

Heinz et al also proposed a force field for fcc metals⁴⁰ compatible with biomolecular force fields (e.g. CHARMM, AMBER, GROMACS), identified a soft epitaxial adsorption mechanism of peptides on noble metal surfaces in solution⁵² as well as contributions to adsorption by induced charges.⁵¹ Corni et al investigated the interaction of peptide molecules with gold {111} surfaces using ab-initio MD.^{S47} A specialized force field to model adsorption of organic molecules on Au {111} surfaces was derived (GoIP)⁴² and applied to study the interaction of Au {111} surfaces with single amino acids.^{S48} The model requires fixed Au atoms and leads to similar results as CHARMM-METAL.^{S41,40,53} Van der Vegt et al. carried out ab-initio and classical simulations of interactions of amino acids with Ni {111} surfaces^{S49} using a specialized force field that is not transferable to common harmonic energy expressions. Baskes et al developed Embedded Atom Models (EAM) for metals.^{33,S50,S51} The energy expression differs from harmonic force fields for biomolecules and surface energies cannot be quantitatively reproduced unless further fit parameters are included (MEAM). Tight-binding methods for the simulation of metals can be applied at the local scale and possess similar advantages and limitations as DFT methods (section S1).⁶⁸ A review of various simulation approaches to material-biological interfaces was given by Harding et al.^{S52}

Muthukumar et al. have used coarse grain models in combination with experiment to examine the translocation of a polymer through protein pores in a membrane driven by electric fields.^{S53} Another coarse-grain study explains possible packing pathways of a genome in a bacteriophage.^{S54} De Pablo et al derived coarse-grain models of DNA that reproduce trends in salt-dependent melting, bubble formation and rehybridization, as well as approximate

mechanical properties as a function of salt concentration.^{S55} MD simulations of an idealized coarse grain polymer glass under tension and compression helped explain creep behaviour and stress-induced dynamics.^{S56} The directed assembly of block copolymers on nanopatterned and templated surfaces using MC simulation with coarse grain models was investigated,^{S57} and Heinz et al have shown the feasibility of square patterns of block copolymers of small domain spacing in good correlation with experiment.⁶ Kremer et al achieved microsecond simulations of the dynamics of bisphenol A polycarbonate using coarse grain and atomistic models in combination.^{S58} Winfree et al studied the design of nucleic acid sequence and DNA secondary structure using a free-energy based thermodynamic model,^{S59} and applied the concept to the self assembly of DNA tiles into origami patterns.^{S60} Loverde et al investigated the stability of worm-like micelles using dissipative particle dynamics (DPD) with soft coarse grain models and showed details of the budding and break-up mechanism.^{S61}

These and numerous other studies at the length scale of 1 to 1000 nm indicate a variety of different simulation methods and parameter sets that are applied to solve problems related to control interfacial processes.

S3. The Role of Combination Rules for Thermodynamic Consistency

Thermodynamic consistency focuses on the reproduction of key physical, chemical, and surface properties of every compound included in the force field. Once this goal is achieved, combination rules imitate interfacial properties in good quantitative or semi-quantitative precision compared to measurements. Support for the performance of combination rules comes from existing force fields (PCFF, AMBER, CHARMM, GROMACS, OPLS-AA) and from the new parameters for inorganic compounds in the INTERFACE force field. For example,

computed solid-vapor surface tensions and solid-water interfacial tensions of gypsum agree <5% with experiment (Table 1).

The key challenge thus lies in obtaining thermodynamically consistent parameters for a given compound, i.e., the best possible approximation of the electronic structure by available parameters in the classical energy expression. Once achieved, the compound can instantly interact with other compounds in the simulation using standard combination rules. Thereby, each compound maintains the density, surface energy, interface energy, modulus, and other properties in the simulation, and does usually not require specialized interaction potentials with other compounds. More information follows in section S4.5 and limitations are described in section 4.3.

S4. Derivation of Force Field Parameters in Detail

S4.1. Existing Sources and New Developments. Common approaches to the derivation of parameters have been described in the documentation of earlier force fields.^{14,18-28,38,S1,S36,S37,S40} The arguably oldest sources are discussions by Max Born and John Edward Jones on potentials of ionic and molecular solids that are now commonly used as Lennard-Jones potentials.¹⁵⁻¹⁷ While approaches to nonbond parameters vary widely, the derivation of bonded parameters is similar among harmonic force fields.

The parameterization procedure for compounds in the INTERFACE force field involves a sequence of steps that worked well for the parameterization of over thirty different compounds, including inorganic compounds as well as organic molecules and polymers such as PEO (Figures S1 and S2). A key initial step is the definition of chemically equivalent atoms on the basis of the 3D chemical formula and available X-Ray structures. X-Ray structures, tabulated bond lengths

and angles also serve as a guide for values of $r_{0,ij}$ and $\theta_{0,ijk}$ (see equations 1 and 2 in the main text). Tabulated atomic and ionic diameters across the periodic table aid in the assignment of $\sigma_{0,ii}$,^{60,61} and an initial interpretation of the polarizability guides in the assignment of the nonbond well depth $\varepsilon_{0,ii}$ for each atom type.⁶⁴ Vibration parameters $k_{rn,ij}$, $k_{\theta n,ijk}$, torsion parameters $V_{\varphi n,ijkl}$, $\varphi_{0n,ijkl}$, atomic charges q_i , and also the Lennard-Jones parameters $\sigma_{0,ii}$ and $\varepsilon_{0,ii}$ have often not been associated with a clear physical and chemical rationale in the past. Comparisons of computed properties to readily available experimental data were often missing, parameters relied on quantum-mechanical data without chemical interpretation or analysis of uncertainties, and discrepancies in bulk and surface properties between simulation and experiment up to multiples have been common.^{14,20,21,27,29-33,39-46,S1-S3}

Such uncertainties, however, can be eliminated by clarification of atomic charges q_i ⁵⁸ and by evaluation of computed surface properties of solids in comparison to experiment to assign Lennard-Jones parameters $\sigma_{0,ii}$ and $\varepsilon_{0,ii}$.^{14,40} These steps lead to thermodynamic consistency (Table 2 and Figure 3).

S4.2. Atomic Charges. Atomic charges q_i (see equations 1 and 2) approximate the distribution of electron density and quantify the extent of covalent bonding versus ionic bonding (Figure 3).⁵⁸ Atomic charges are experimentally accessible (Table S1) and must be accurately reproduced in the force field. Else, deviations in computed properties arise that cannot be compensated by fitting other parameters without compromising the quality of the force field.^{14,29-31,41,43,45,46,S2,S3,S5,S6-S13} The dependable assignment of atomic charges has been described in ref. 58 and a decade of practice reinforced its key role for reliable simulations.

In short, several methods are suited to deliver appropriate atomic charges and validate their accuracy.⁵⁸ (1) X-Ray deformation densities^{S19-S25} in combination with Hirshfeld partitioning of the measured electron density into spherical atomic basins⁶² yield the best atomic charges for molecular simulations (Table S1). These charges, in combination with van-der-Waals parameters and bonded parameters, typically reproduce dipole moments, cleavage energies, polar contributions to interface tensions, and heats of immersion in agreement with measurements. (2) Similarly, dipole moments yield atomic charges or charges on groups of atoms for many compounds across the periodic table.⁶⁰ The atomic charges from dipole moments are consistent with the charges from X-Ray deformation densities and suitable for molecular simulations. (3) An extended Born model, in association with trends in chemical properties for a set of related compounds across the periodic table, also provides consistent atomic charges, especially if no direct experimental data are available. This method can be as precise as $\pm 0.1e$ and involves a quantitative analysis of covalent and ionic contributions to chemical bonds in a given compound based on available thermochemical data and the coordination environment. Thermochemical data include atomization energies, ionization potentials, and electron affinities, which are readily available for all elements.⁶⁰ The development of density functionals for QM calculations has meanwhile adopted similar practices of referencing thermochemical data.¹⁰ In combination with methods 1 and 2, this approach is fast and accurate for any compound across the periodic table, and entirely based on reported, reproducible chemical insight.⁵⁸ (4) Quantum-mechanical methods must be used with caution (Figure 3a). The derivation of absolute values of atomic charges is not recommended due to possible large deviations.^{58,63,S26} The estimation of relative atomic charges from one compound to another becomes more reliable (i) if the atomic charges

for one compound are exactly known and (ii) if high level basis functions/density functionals are employed.

Atomic charges can be determined within approximately $\pm 5\%$ uncertainty, higher precision is typically not possible related to the anisotropy of the electron density. It is critical, however, to minimize the error, as the sensitivity of interfacial properties, folding of chain molecules, and phase transition temperatures, for example, to the chosen atomic charges is very high in molecular simulations.

Some examples illustrate this sensitivity. (1) Small deviations from appropriate charges in polyethylene oxide at 20 °C (Figure 3a) would lead to phase separation of the polymer in water as opposed to a homogenous solution known from laboratory observations. (2) Atomic charges of Si in tetrahedral O coordination in silicates have been subject to very high uncertainty from +0.5e to +4.0e in various models,^{29-31,41,43,45,46,58,S2,S3,S5,S7-S13} which lead to a spread in computed surface energies up to 100-fold unless the correct value +1.1e ($\pm 0.1\text{e}$) is employed.¹⁴ (3) Similar discrepancies are common for Al in octahedral oxygen coordination and many more minerals.⁵⁸ At times, both charges and the surface structure may be misrepresented in models, such as titania surfaces with dangling oxygen bonds in aqueous solution.⁴⁵ (4) Misleading atomic charges using DFT calculations and arbitrary charge partitioning schemes are also reported in other recent parameterizations of silica and silicate hydrates.^{43,46} Associated deviations in interfacial energies then scale with the square of q_i , distort water layering on surfaces, and conformations of adsorbed molecules. Conclusions from simulations using such parameters are questionable and often resonate poorly in the experimental community.⁴³

S4.3. Van-der-Waals Parameters. While the correct polarity ensures an appropriate amount of electrostatic contributions to cohesive energies and interfacial energies, the balance between

Coulomb energies, short-range repulsion, and mid-range attractive van-der-Waals energies is equally important and depends on the parameters $\sigma_{0,ii}$ and $\varepsilon_{0,ii}$ (equations 1 and 2). The nonbond diameter $\sigma_{0,ii}$ reflects the size of the atom or ion and is known across the periodic table.^{60,61} The well depth $\varepsilon_{0,ii}$ reflects the atomic polarizability, expressed via summation of pairwise interactions. Values of $\varepsilon_{0,ii}$ are exactly known for rare gases and Halgren suggested that $\varepsilon_{0,ii}$ increases within a row of the periodic table toward the values for the corresponding rare gas.⁶⁴ In addition, the well depth $\varepsilon_{0,ii}$ depends (i) on the charge state of the atom which changes the polarizability (higher $\varepsilon_{0,ii}$ for negatively charged atoms) and (ii) on the volume density of covalent bonds in the vicinity of the atom, as the cohesion between molecules or surfaces is represented by the values $\varepsilon_{0,ii}$ and by the number of pairwise interactions per unit volume. The latter condition requires smaller $\varepsilon_{0,ii}$ in a dense covalent framework compared to the same atom in small molecules or ions. These factors are not simple to quantify, and therefore a final adjustment of the well depths $\varepsilon_{0,ii}$ to reproduce surface tensions, hydration energies, cleavage energies, and other available surface data is essential (Figure 3b). Equally, a physically consistent interpretation of the values $\varepsilon_{0,ii}$ is important, especially when $\varepsilon_{0,ii}$ values for several atom types need to be determined.

In detail, the interpretation of $\varepsilon_{0,ii}$ involves an initial assessment of $\varepsilon_{0,ii}$ in the context of Halgren's principle within the periodic table, then in the context of the charge state of the atom, and then in the context of the volume density of covalent bonds. Further comparison of suitable $\varepsilon_{0,ii}$ values with $\varepsilon_{0,ii}$ values of the same element in related compounds is highly recommended. As values of $\varepsilon_{0,ii}$ are the most "adjustable" parameters in the force field, it is recommended to check the sensitivity of computed surface properties (e.g. cleavage energy for a solid, cohesive

energy for a liquid) across a range of possible values of $\varepsilon_{0,ii}$ (Figure S2). For example, systematic variations of $\varepsilon_{0,ii}$ across one order of magnitude for a few slightly different settings of $\sigma_{0,ii}$ each and analysis of a simple computed surface property satisfy this condition. The final assignment of $\varepsilon_{0,ii}$ for each atom type i should be accompanied by a full rationale. For a thermodynamically consistent parameterization, it is then often found that a change in $\varepsilon_{0,ii}$ by $\pm 5\%$ does not significantly affect the performance of the force field.

Nonbond diameters $\sigma_{0,ii}$ deviate usually $\pm 5\%$ from book value^{60,61} as their interpretation is straightforward. Therefore, their priority in the parameterization is rather low (Table 2) and small adjustments are made to reproduce the experimentally determined density in the simulation. More discussion can be found in ref. 14.

S4.4. Bonded Parameters. Bonded parameters are needed for bond, angle, torsion, and out-of-plane potentials (equations 1 and 2). The assignment of accurate torsion parameters $V_{\varphi_{0n,ijkl}}$ and $\varphi_{0n,ijkl}$ is essential to reproduce conformation equilibria of molecules and folding of chain molecules such as proteins in a simulation. Minerals usually require no torsion and no out of plane parameters (equal zero).¹¹ The energy profile during bond rotation, when applicable, involves the superposition of nonbond interactions and bonded interactions. Therefore, the torsion potential serves as an add-on to tune other interactions that are already in place. The derivation of parameters $V_{\varphi_{0n,ijkl}}$ and $\varphi_{0n,ijkl}$ for each dihedral angle first requires insight into target values of equilibrium dihedral angles and torsion barriers. These target values are best derived according to (i) experiment (IR, NMR), (ii) stereochemical knowledge and analogies to similar compounds, (iii) quantum-mechanical calculations with appropriate high-level basis sets

or density functionals. The second step is the assignment of parameters in the torsion potential for every dihedral angle to match the energy profile to the chosen target values.

In detail, the assignment of constants $V_{\varphi n,ijkl}$ and $\varphi_{0n,ijkl}$ for each dihedral angle involves (i) an analysis of the torsion profile in the absence of torsion parameters (all $V_{\varphi n,ijkl}$ equal zero), (ii) adjustments in torsion parameters to match the target energy profile, and (iii) testing of the new energy profile using MD simulations of the relevant portion of the chain molecule. To begin, a 5 ns MD simulation of the relevant torsion fragment including first and second bonded neighbors is carried out in vacuum (or in solution, respectively), recording snapshots every 10 fs. A distribution plot of the dihedral angles $A(\varphi)$ is then prepared and converted into a logarithmic plot $E(\varphi) = -RT \ln A(\varphi) + C$ to determine the torsion barriers and equilibrium dihedral angles in the absence of any torsion potential. Then, the barrier heights $V_{\varphi n,ijkl}$ and the angular offsets $\varphi_{0n,ijkl}$ in the trigonometric torsion potential (equations 1 and 2) are edited to match the target values. Finally, the MD simulation is repeated with the new torsion potential to verify the reproduction of target angular minima and energy barriers in the torsion energy profile.

Current torsion potentials for biomolecules such as in CHARMM and AMBER reproduce folding of DNA and proteins up to tens of monomers in length.^{S35,S36} Yet torsion potentials may undergo further possible improvements (1) in the accuracy of torsion barriers and equilibrium angles, (2) specifically in the representation of stereoelectronic effects (e. g. in polyethylene oxide and carbohydrates), (3) and related to the dependence on pH in charged chain molecules. For example, significant differences were found in computed equilibrium angles Φ , Ψ as well as in torsion barriers for short homopeptides (Ser_3 , Tyr_3) using different force fields such as CHARMM and CVFF.⁵⁴ Also, the eclipsed rotation barrier of *n*-butane of 3.95 kcal/mol in the gas phase according to IR spectroscopy^{S62} still amounts to 5 to 6 kcal/mol in some force fields

based on older quantum-mechanical results. The higher barrier slows down rotation dynamics in hydrocarbons up to a factor of 30 at room temperature according to the Boltzman factor.

Therefore, the capabilities of force fields to study folding of proteins, DNA, and polyelectrolytes are currently still not fully exploited. Torsion potentials often still rely on partially verified assumptions or “fits” rather than on the interpretation of torsion barriers, as the case of *n*-butane shows. The maximum length of peptides to compute conformations and folding in agreement with experiment is $\sim 10^1$ amino acids in solution. Improved rotation barriers, validated specifically in solution, could enable dependable simulations of folding and self-organization of proteins as long as $\sim 10^2$ amino acids. Examples for the simulation of folding of selected longer chains ($>>10$ amino acids) in very good agreement with experiment have been reported,⁵³⁵ however, the results do not imply reliability for other sequences, nor even for the same sequence under different pH, temperature, solvent, and ionic strength using current parameters.

A starting point for the derivation of parameters for bonds ($k_{r,ij}$, $r_{0,ij}$) and angles ($k_{\theta,ijk}$, $\theta_{0,ijk}$) are crystal structures of the mineral, metal, or molecular crystal determined by X-Ray or neutron diffraction, as well as compilations of bond lengths and angles for compounds across the periodic table (Table 2).⁶⁰ Experimentally determined equilibrium bond lengths $r_{0,ij}$ and angles $\theta_{0,ijk}$ can directly be used in the force field. Sometimes minor adjustments due to the additional influence of nonbond interactions become necessary (<5%), for example, when minerals with strong ionic attraction require a slightly higher $r_{0,ij}$ to help offset strong cohesion.

Initial approximations of harmonic force constants $k_{r,ij}$ and $k_{\theta,ijk}$ can be made according to corresponding frequencies in experimental IR and Raman spectra, and by comparison to bonds and angles in similar compounds. Initial parameter choices are then tested by computation of the

IR/Raman spectrum, which involves a short MD simulation (5 ps with recording of coordinates every time step of 1 fs),¹⁴ calculation of the velocity autocorrelation function and Fourier transformation. The force constants are then adjusted until computed vibration frequencies match experiment as closely as possible (see ref. 14 for details). The feasible accuracy in frequencies is usually better than 50 cm⁻¹, while intensities are not reproducible due to neglect of the full electronic structure.

S4.5. Interfaces and Multiphase Materials. For the simulation of interfaces, Lennard-Jones parameters for interactions between different atom types are obtained from parameters for homoatomic interactions (σ_{ij} and ε_{ij} from $\sigma_{0,ii}$, $\sigma_{0,jj}$, $\varepsilon_{0,ii}$, $\varepsilon_{0,jj}$) and reliance on standard combination rules. Thermodynamic consistency for all compounds enables the accurate simulation of mixtures of liquids, solid-liquid interfaces, co-crystals, and multi-component composites. For example, the reliable computation of mineral-water interface tensions is a result of using parameters that yield the surface tension of the solid mineral phase and the surface tension of liquid water in agreement with experiment. Addition of a polyelectrolyte to the solid-liquid interface enables a similarly dependable computation of the adsorption energy, if the parameters of the polyelectrolyte are thermodynamically consistent and reproduce the hydration energy of the polyelectrolyte in agreement with experiment.

It is characteristic that thermodynamically consistent parameters lead to very good agreement of many computed properties with experiment that were not originally fitted. For example, such properties include surface energy anisotropies, surface reconstruction processes, dielectric properties, heat capacity, thermal conductivity, diffusion constants, and elastic constants. Also sensitive properties such as phase transition temperatures (in a range of ± 200 K from the

reference state) and radii of gyration of chain molecules agree well with experiment, such as for the model of polyethylene(oxide) in the INTERFACE force field.

The derivation of force field parameters for organic molecules, solvents, and biopolymers requires the same rigorous assessment as for inorganic compounds. This includes, for example, surface tensions, vaporization energies of liquids at room temperature, short-range molecular orientation (including pi-stacking interactions), and hydration energy.

S4.6. Available Versions of the INTERFACE Force Field and Adaptation to Other Force Field Expressions. All parameters are provided in INTERFACE-PCFF format as part of the Supporting Information. The versions INTERFACE-CHARMM and INTERFACE-CVFF are also available for several compounds. The INTERFACE force field can also be appended to any existing force field based on a harmonic energy expression. Proper interfacing with a different harmonic force field involves all parameters as given in INTERFACE-PCFF (or INTERFACE-CHARMM) format with appropriate adjustments in LJ parameters as described in section 2.2 (no torsion parameters needed for minerals).

The adjustment of LJ parameters (if necessary) first involves a qualitative estimate of the direction and magnitude of changes, guided by known examples for the conversion of LJ parameters from one harmonic force field to another.^{14,40,47,48} Second, a comparison of computed cell parameters to values from experiment (or to values by the original force field) is carried out to test and refine the new LJ parameters until a good fit is achieved. Third, a surface property such as cleavage energy, hydration energy, or cohesive energy is computed using the new force field to probe quantitative equivalence with the original force field (differences in single point energies for two different configurations of the same system may suffice for comparison of original and new force field, rather than obtaining full dynamic data). Usually, a good result is

expected without further adjustments, otherwise the respective part of the original parameterization procedure is followed to optimize the parameters for the new energy expression (sections 3.3. and S4.3., Figures 3b and S2).

Secondary validation of further properties, e.g., mechanical, can also be helpful depending on purpose. The adaptation procedure is straightforward and easier than previous transferability protocols that sometimes also modify atomic charges.

S4.7. Parameterization of New Compounds. Parameters for novel compounds can be obtained using the procedure toward thermodynamically consistent parameters (Figure S2) whereby existing compounds provide helpful benchmarks. The INTERFACE parameterization for a single compound may require a few weeks for experienced users up to several months for less experienced users and consumes 10^3 to 10^4 CPU hours, including the collection of charges and performance of MD simulations to refine parameters until convergence of a variety of properties and agreement with experiment is achieved. Major efforts involve the assignment of atomic charges and often the retrieval of unequivocal experimental reference data (Figure 3).

The procedure also provides parameters for compounds without known experimental or tabulated data in very good approximation. The assignment of initial justified charges and thermodynamically consistent other parameters according to the protocol, in comparison to chemically similar compounds as well as to QM data, provides the best chances for an accurate initial parameterization. For example, cement minerals were initially parameterized in this way, only by help of available X-Ray data and comparison to layered silicates. Retrieval of experimental data for cleavage energies of tricalcium silicate and surface energies of tobermorite from experimental sources at a later time and comparison to computed values required only minor or no adjustments. The same was true for the initial quality of computed mechanical

properties. Ultimately, any parameterization protocol faces the challenge that validation of the force field requires experimental verification of computed predictions and, possibly, iterative improvements.

Secondary validation by computation of a larger array of properties, such as extensive adsorption, mechanical, and thermal data requires additional time. Secondary validation usually confirms expected uncertainties from primary validation and parameter revisions are minor or unnecessary. A consistent interpretation of the parameters for a new compound in the context of existing parameters for similar compounds also allows estimates of uncertainty and reduces the need for extensive secondary validation.

S5. Further Validation and Possible Extensions

S5.1. Reliability of LJ Parameters for FCC Metals. Before ref. 40, LJ parameters for metals were fitted to densities at 298 K and vaporization energies near 3000 K, which leads to poor performance with respect to many properties.^{20,21,27,S4,S6} In ref. 40, we have chosen LJ parameters that reproduce the density at 298 K and the experimentally known surface energy at 298 K, i.e., following thermodynamic consistency, which eliminates many deviations and turns LJ potentials into well-performing models for fcc metals. In addition to densities and surface tensions that are fitted through the choice of $\sigma_{0,ii}$ and $\varepsilon_{0,ii}$, surface energy anisotropies for different facets,⁴⁰ metal-water interface tensions, and the dielectric constant of the first three molecular layers of water adsorbed on gold ($\varepsilon_R = 6, 32, 78$) agree with measurements down from errors by multiples using previous LJ potentials.^{40,51} Also, adsorption energies of peptides and surfactants on even {h k l} metal surfaces in solution are consistent with results by phage display and measured adsorption energies.⁵²⁻⁵⁴ Trends in molecule adsorption and specificity to

shaped metal surfaces agree with experimental studies,⁵⁴ and elastic constants in 12-6 potentials agree ~20% with experiment, sometimes even better than 5% as shown for Pd (see Table 1).⁴⁰

Further, the critical size of Pd metal nanoclusters for the transition from amorphous to crystalline at ~1.5 nm is predicted in agreement with TEM and XRD studies.⁵⁵

In particular, a growing number of studies by many research teams provide further evidence for the applicability and accuracy of the models. For example, Petkov et al. found very good agreement between experimentally measured and computed pair correlation functions for Au-Pt alloy nanoparticles of various compositions and insight into local disorder.^{S63} Saiz-Poseu et al. investigated the self-assembly of catechol-based macrocycles on gold {111} surfaces by XPS, STM, and molecular dynamics simulation and identified the influence of solute versus solvent in very good agreement of simulations with measurements.^{S64} Other simulations employed the models to investigate the influence of molecular adsorption on elongating gold nanowires,^{S65} to predict the morphology of self-assembled nanoparticles in diblock copolymers,^{S66} to analyze the structure and dynamics of thiol-functionalized gold nanoparticles in aqueous environment,^{S67} and the possible mechanism of formation of alkanethiol monolayers on gold.^{S68} The parameters for aluminum were also employed in a mesoscale model of electrode interfaces in Li-ion batteries.^{S69} Schatz et al. examined transitions in DNA from A to B form between gold surfaces.^{S70} The parameters for Cu and Au were used in conjunction with DFT calculations to examine interactions of small water clusters with metal surfaces in detail.^{S71,72} Kim et al. used the models in Monte Carlo simulation to explain water meniscus condensation and capillary forces in AFM on gold surfaces.^{S73} Molecular dynamics simulations by Barone et al. provide insight into the self-assembly of tetraphenylporphyrin-based monolayers and bilayers on silver surfaces.^{S74}

S5.2. Layered Silicates. Beyond our own initial studies, the parameters for layered silicates have been used for simulations by various research teams and shown valuable correlations with a broad range of experimental data. For example, Fermeglia, Prich, and Posocco et al. carried out multiscale simulations of montmorillonite/poly(ethylene oxide) nanocomposites with atomistic detail^{S75} as well as simulations of silylated montmorillonites of different chain length to explain trends in basal plane spacing from X-ray data and the role of silane spacers.^{S76} Cummings et al. carried out simulations of confined liquids between mica layers,^{S77} examined fluid-solid transitions of various confined species,^{S78,S79} and investigated the effect of electric fields on water in mica pores.^{S80} In studies by Pandey et al., the parameters for layered silicates were used to derive coarse grain models for clay minerals and examine the adsorption of peptides.^{S81} Mathew and Luthey-Schulten investigated the influence of the montmorillonite surface on nucleotide oligomerization reactions.^{S82} Jordan et al. showed very good agreement of computed structural properties by the force field in comparison to DFT results.^{S83} Wallis et al. investigated the interlayer structure of montmorillonite containing iron cations and its relation to catalytic activity in oxidative coupling reactions of hydrophobic organic substrates.^{S84} The adsorption of polycyclic aromatic heterocycles on pyrophyllite using the force field and DFT methods was investigated by Sainz-Diaz et al.^{S85} Xu et al. investigated the Young's modulus of effective clay clusters in polymer nanocomposites^{S86} and Berkowitz et al. analyzed restructuring of surfactants on mica surfaces in aqueous solution by molecular dynamics simulation.^{S87}

The procedure to assign atomic charges for various minerals and organic compounds has also been used in many instances by other research teams (not further specified here).^{S8} Although a rigorous algorithmic implementation has not yet been implemented to-date, physical-chemical

principles reported in this procedure (summarized in Figure 3a) are the key to parameter developments in the INTERFACE force field.

S5.3. Comparison with Reactive Potentials and Other Potential Types. As mentioned in section 4.3., the INTERFACE force field cannot describe chemical reactions in its present form, except some special cases such as hydration of plaster of Paris to gypsum, photoisomerization reactions,⁶⁷ the abstraction of metal atoms from the surface of metal nanoparticles in catalytic reactions, or the dissolution of certain ionic species such as alkali, phosphate, and sulfate on surfaces. However, the simplicity of the potential supports extensions to Morse potentials, for example, to model the dissociation of covalent bonds. Such extensions do not fully compromise the use of parameters for biopolymers and organic molecules, as is the case in dedicated reactive force fields. Other possibilities to trace chemical reactions include the combination of the INTERFACE force field with quantum methods on a local scale, the simplified or stepwise simulation of reactions using customized force field parameters for reaction intermediates.

Reactive force fields work well for certain classes of compounds, e.g., ReaxFF is suited for reactions of hydrocarbons³⁴ and AIREBO for carbon compounds.³⁷ A caveat for other compounds is that computed surface properties of reactants or products themselves may deviate considerably from experiment, e.g., surface tensions, hydration energies, or interfaces with water and biomolecules. Moreover, the simulation of interfaces with biopolymers and other phases is difficult due to the lack of parameters in the dedicated format.^{34,37} Therefore, simple customized reactive extensions of the INTERFACE force field based on QM and experimental data for non-reactively parameterized compounds have the potential to yield good results due the focus on accurate properties and few, well defined parameters.

In comparison to embedded atom potentials for metals, the INTERFACE force field is a possible alternative due to the outstanding performance for fcc metals (section S5.2). Further extensions of the INTERFACE parameters may comprise polarizability (for induced charges) and coverage of non-fcc metal structures.

In conclusion, we emphasize that every potential possesses strengths and weaknesses. The INTERFACE force field and harmonic energy expressions are one class among different functional forms of which each provides valuable insight for a certain range of systems and conditions of state.

S6. One-Page Overview of the INTERFACE Force Field

Thermodynamically consistent parameters for inorganic and organic compounds (Table 1) have been integrated in harmonic force fields for organic and biological compounds and compiled as a first version of the INTERFACE force field. The attached INTERFACE-PCFF force field contains parameters added into PCFF (equation 2) as well as molecular models for the following compounds:

- **Layered silicates:** mica, different montmorillonites, pyrophyllite, including surfaces of different CEC and cation distributions according to NMR data
- **Fcc metals:** Ag, Al, Au, Cu, Ni, Pb, Pd, Pt, including {111}, {100}, and {110} surfaces
- **Silica:** bulk minerals as well as surfaces of different degree of ionization for specific pH values and particle sizes
- **Calcium sulfates:** calcium sulfate hemihydrate and gypsum, including different cleavage planes
- **Cement minerals:** tricalcium silicate, tricalcium aluminate, ettringite, monosulfate, tobermorite 11 Å, tobermorite 14 Å, including different cleavage planes
- **Hydroxyapatite:** bulk mineral and different cleavage planes
- **Poly(ethylene oxide):** crystal and polymer chain including gauche effect and approximate solubility (radius of gyration) in water

All models are individually explained in the documentation and ready to use in MD simulations, for example, using Discover, Forcite, and LAMMPS programs. Versions of equivalent force fields, such as INTERFACE-CHARMM, INTERFACE-CVFF, are completed for several compounds.

S7. Additional References

- (S1) (a) Sun, H.; Mumby, S. J.; Maple, J. R.; Hagler, A. T. *J. Am. Chem. Soc.* **1994**, *116*, 2978-2987. (b) Maple, J. R., Thacher, T. S., Dinur, U.; Hagler, A. T. *Chem. Des. Autom. News* **1990**, *5*, 5-10. (c) Sun, H. *J. Comput. Chem.* **1994**, *15*, 752-768. (d) Hill, J.-R.; Sauer, J. *J. Phys. Chem.* **1994**, *98*, 1238 - 1244. (e) Sun, H. *Macromolecules* **1995**, *28*, 701-712.
- (S2) Beest, B. W. H.; Kramer, G. J.; Van Santen, R. A. *Phys. Rev. Lett.* **1990**, *64*, 1955-1958.
- (S3) Collins, D. R.; Catlow, C. R. A. *Am. Mineral.* **1992**, *77*, 1172-1181.
- (S4) Shu, Z.; Davies, G. J. *Phys. Status Solidi A* **1983**, *78*, 595-605.
- (S5) Sanders, M. J.; Leslie, M.; Catlow, C. R. A. *J. Chem. Soc., Chem. Comm.* **1984**, 1271-1273.
- (S6) Uppenbrink, J.; Wales, D. J. *J. Chem. Phys.* **1992**, *96*, 8520-8534.
- (S7) Hill, J. R.; Sauer, J. *J. Phys. Chem.* **1994**, *98*, 1238-1244.
- (S8) Hill, J. R.; Sauer, J. *J. Phys. Chem.* **1995**, *99*, 9536-9550.
- (S9) Teppen, B. J.; Rasmussen, K.; Bertsch, P. M.; Miller, D. M.; Schafer, L. *J. Phys. Chem. B* **1997**, *101*, 1579-1587.
- (S10) Cygan, R. T.; Liang, J. J.; Kalinichev, A. G. *J. Phys. Chem. B* **2004**, *108*, 1255-1266.
- (S11) Wang, J. W.; Kalinichev, A. G.; Kirkpatrick, R. J.; Cygan, R. T. *J. Phys. Chem. B* **2005**, *109*, 15893-15905.
- (S12) Lopes, P. E. M.; Murashov, V.; Tazi, M.; Demchuk, E.; MacKerell, A. D. *J. Phys. Chem. B* **2006**, *110*, 2782-2792.
- (S13) Cruz-Chu, E. R.; Aksimentiev, A.; Schulten, K. *J. Phys. Chem. B* **2006**, *110*, 21497-21508.

- (S14) (a) Brunauer, S.; Kantro, D. L.; Weise, C. H. *Canadian J. Chem.* **1956**, *31*, 729-742. (b) Westwood, A. R. C.; Goldheim, D. L. *J. Appl. Phys.* **1963**, *34*, 3335-3339. (c) Boumiz, A.; Sorrentino, D.; Vernet, C.; Tenoudji, F. C. in *13th Proceedings of the 2nd RILEM Workshop on Hydration and Setting: Why does cement set? An interdisciplinary approach*, Nonat, A., ed.; Dijon, France, 1997.
- (S15) Brunauer, S.; Kantro, D. L.; Weise, C. H. *Canadian J. Chem.* **1959**, *37*, 714-724.
- (S16) (a) Taylor, J. A. G.; Hockey, J. A. *J. Phys. Chem.* **1966**, *70*, 2169-2172. (b) Lamb, R. N.; Furlong, D. N. *J. Chem. Soc., Faraday Trans. 1*, **1982**, *78*, 61-73.
- (S17) (a) Dundon, M. L.; Mack, E., Jr. *J. Am. Chem. Soc.* **1923**, *45*, 2479-2485. (b) Kimura, O. *Bull. Chem. Soc. Jpn* **1942**, *17*, 61-64. (c) Oglesby, M. L.; Gutshall, P. L.; Phillips, J. M. *American Mineralogist* **1976**, *61*, 295-298. (d) Söhnel, O. *J. Crystal Growth* **1982**, *57*, 101-108. (e) Weijnen, M.P.C.; van Rosmalen, G. M.; Bennema, P.; Rijpkema, J. J. M. *J. Crystal Growth* **1987**, *82*, 509-527.
- (S18) The cleavage energy of hydroxyapatite, $\text{Ca}_{10}(\text{PO}_4)_6(\text{OH})_2$ is lower than 1180 mJ/m^2 for $\text{Ca}(\text{OH})_2$, ref. S14a, due to the presence of phosphate ions of lower polarity. The cleavage energy is also higher than 360 mJ/m^2 for $\text{CaSO}_4 \cdot 2 \text{ H}_2\text{O}$, ref. S17a, related to the absence of crystal water and higher polarity of phosphate versus sulfate ions.
- (S19) (a) Brill, R.; Hermann, C.; Peters, C. *Z. Anorg. Allg. Chem.* **1948**, *257*, 151-165. (b) Witte, H.; Wölfel, E. *Rev. Mod. Phys.* **1958**, *30*, 51-55. (c) Aref'ev, K. P.; Vorob'ev, S. A. *Izv. Vuz. Fiz.* **1972**, *15*, 34-38. (d) Hill, R. J. *J. Phys. Chem. Miner.* **1979**, *5*, 179-200.
- (S20) (a) Thong, N.; Schwarzenbach, D. *Acta Crystallogr., Sect. A* **1979**, *A35*, 658-664. (b) Göttlicher, S.; Knöchel, C. D. *Acta Crystallogr., Sect. B* **1980**, *B36*, 1271-1277.

- (S21) Lewis, J.; Schwarzenbach, D. *Acta Crystallogr., Sect. A: Cryst. Phys., Diff., Theor., Gen. Crystallogr.* **1982**, *A38*, 733-739.
- (S22) (a) Hermansson, K.; Thomas, J. O. *Acta Crystallogr., Sect. C* **1983**, *C39*, 930-936. (b) Greenwood, N. N.; Earnshaw, A. *Chemistry of the Elements*; Pergamon Press: Oxford, 1984.
- (S23) Vaalstra, T. P.; Maslen, E. N. *Acta Crystallogr., Sect. B* **1987**, *B43*, 448-454.
- (S24) Wood, J. S. *Inorg. Chim. Acta* **1995**, *229*, 407-415.
- (S25) Belokonewa, E. L.; Gubina, Yu. K.; Forsyth, J. B.; Brown, P. J. *J. Phys. Chem. Min.* **2002**, *29*, 430-438.
- (S26) (a) Mulliken, R. S. *J. Chem. Phys.* **1955**, *23*, 1833-1840. (b) Bader, R. F. W. *Chem. Rev.* **1991**, *91*, 893-928.
- (S27) Atkins, P. W.; Friedman, R. S. *Molecular Quantum Mechanics*, 3rd ed.; Oxford University Press: Oxford, 1997.
- (S28) McQuarrie, D. A.; Simon, J. D. *Physical Chemistry – A Molecular Approach*; University Science Books: Sausalito, CA, 1997.
- (S29) *Springer Handbook of Atomic, Molecular, and Optical Physics*, Drake, G. W. F., ed.; Springer, New York, 2006.
- (S30) Krack, M.; Parrinello, M. *Phys. Chem. Chem. Phys.* **2000**, *2*, 2105-2112.
- (S31) Valero, R.; Gomes, J. R. B.; Truhlar, D. G.; Illas, F. *J. Chem. Phys.* **2010**, *132*, 104701.
- (S32) Jacquemin, D.; Perpete, E. A.; Ciofini, I.; Adamo, C.; Valero, R.; Zhao, Y.; Truhlar, D. G. *J. Chem. Theory Comput.* **2010**, *6*, 2071-2085.

- (S33) Westmoreland, P. R.; Kollman, P. A.; Chaka, A. M.; Cummings, P. T.; Morokuma, K.; Neurock, M.; Stechel, E. B.; Vashishta, P. *Applying Molecular and Materials Modeling: An International Comparative Study*; Kluwer Academic, Amsterdam, 2002.
- (S34) Jaguar Program and Graphical Interface. Schrodinger, Inc. 2012.
- (S35) Lindorff-Larsen, K.; Piana, S.; Dror, R. O.; Shaw, D. E. *Science* **2011**, *334*, 517-520.
- (S36) MacKerell, A. D., Jr.; Feig, M.; Brooks, C. L., III *J. Comput. Chem.* **2004**, *25*, 1400-1415.
- (S37) Nath, S. K.; Escobedo, F. A.; de Pablo, J. J. *J. Chem. Phys.* **1998**, *108*, 9905-9911.
- (S38) Harmandaris, V. A.; Adhikari, N. P.; van der Vegt, N. F. A.; Kremer, K. *Macromolecules* **2006**, *39*, 6708-6719.
- (S39) Nielsen, S. O.; Lopez, C. F.; Srinivas, G.; Klein, M. L. *J. Chem. Phys.* **2003**, *119*, 7043-7049.
- (S40) Monticelli, L.; Kandaswamy, S. K.; Periole, X.; Larson, R. G.; Tielemans, D. P.; Marrink, S. J. *J. Chem. Theory Comput.* **2008**, *4*, 819-834.
- (S41) Pandey, R. B.; Heinz, H.; Feng, J.; Farmer, B. L.; Slocik, J. M.; Drummy, L. R.; Naik, R. R. *Phys. Chem. Chem. Phys.* **2009**, *11*, 1989-2001.
- (S42) Groot, R. D.; Warren, P. B. *J. Chem. Phys.* **1997**, *107*, 4423-4435.
- (S43) Fraaije, J. G. E. M.; vanVlimmeren, B. A. C.; Maurits, N. M.; Postma, M.; Evers, O. A.; Hoffmann, C.; Altevogt, P.; GoldbeckWood, G. *J. Chem. Phys.* **1997**, *106*, 4260-4269.
- (S44) Feng, X. L.; Marcon, V.; Pisula, W.; Hansen, M. R.; Kirkpatrick, J.; Grozema, F.; Andrienko, D.; Kremer, K.; Mullen, K. *Nature Mater.* **2009**, *8*, 421-

- (S45) Machesky, M. L.; Predota, M.; Wesolowski, D. J.; Vlcek, L.; Cummings, P. T.; Rosenqvist, J.; Ridley, M. K.; Kubicki, J. D.; Bandura, A. V.; Kumar, N.; Sofo, J. O. *Langmuir* **2008**, *24*, 12331-12339.
- (S46) Zhao, X. C.; Striolo, A.; Cummings, P. T. *Biophysical J.* **2005**, *89*, 3856-3862.
- (S47) Calzolari, A.; Cicero, G.; Cavazzoni, C.; Di Felice, R.; Catellani, A.; Corni, S. *J. Am. Chem. Soc.* **2010**, *132*, 4790-4795.
- (S48) Hoefling, M.; Iori, F.; Corni, S.; Gottschalk, K. E. *Langmuir* **2010**, *26*, 8347-8351.
- (S49) Schravendijk, P.; Ghiringhelli, L. M.; Delle Site, L.; van der Vegt, N. F. A. *J. Phys. Chem. C* **2007**, *111*, 2631-2642.
- (S50) Baskes, M. I.; Melius, C. F. *Phys. Rev. B* **1979**, *20*, 3197-3204.
- (S51) Baskes, M. I. *Phys. Rev. Lett.* **1999**, *83*, 2592-2595.
- (S52) Harding, J. H.; Duffy, D. M.; Sushko, M. L.; Rodger, P. M.; Quigley, D.; Elliott, J. A. *Chem. Rev.* **2008**, *108*, 4823-4854.
- (S53) Wong, C. T. A.; Muthukumar, M. *J. Chem. Phys.* **2010**, *133*, 045101.
- (S54) Forrey, C.; Muthukumar, M. *Biophysical J.* **2006**, *91*, 25-41.
- (S55) Knotts, T. A.; Rathore, N.; Schwartz, D. C.; de Pablo, J. J. *J. Chem. Phys.* **2007**, *126*, 084901.
- (S56) Riggleman, R. A.; Schweizer, K. S.; de Pablo, J. J. *Macromolecules* **2008**, *41*, 4969-4977.
- (S57) Detcheverry, F. A.; Liu, G. L.; Nealey, P. F.; de Pablo, J. J. *Macromolecules* **2010**, *43*, 3446-3454.
- (S58) Hess, B.; Leon, S.; van der Vegt, N.; Kremer, K. *Soft Matter* **2006**, *2*, 409-414.
- (S59) Dirks, R. M.; Lin, M.; Winfree, E.; Pierce, N. A. *Nucl. Acids Res.* **2004**, *32*, 1392-1403.

- (S60) Fujibayashi, K.; Hariadi, R.; Park, S. H.; Winfree, E.; Murata, S. *Nano Lett.* **2008**, *8*, 1791-1797.
- (S61) Loverde, S. M.; Ortiz, V.; Kamien, R. D.; Klein, M. L.; Discher, D. E. *Soft Matter* **2010**, *6*, 1419-1425.
- (S62) Herrebout, W. A.; van der Veken, B. J.; Wang, A.; Durig, J. R. *J. Phys. Chem.* **1995**, *99*, 578-585.
- (S63) Petkov, V.; Wanjala, B. N.; Loukrakpam, R.; Luo, J.; Yang, L.; Zhong, C. J.; Shastri, S. *Nano Letters* **2012**, *12*, 4289-4299.
- (S64) Saiz-Poseu, J.; Martinez-Otero, A.; Roussel, T.; Hui, J. K. H.; Montero, M. L.; Urcuyo, R.; MacLachlan, M. J.; Faraudo, J.; Ruiz-Molina, D. *Phys. Chem. Chem. Phys.* **2012**, *14*, 11937-11943.
- (S65) French, W. R.; Iacovella, C. R.; Cummings, P. T. *J. Phys. Chem. C* **2011**, *115*, 18422-18433.
- (S66) Posocco, P.; Posel, Z.; Fermeglia, M.; Lisal, M.; Prich, S. *J. Mater. Chem.* **2010**, *20*, 10511-10520.
- (S67) Heikkila, E.; Gurtovenko, A. A.; Martinez-Seara, H.; Hakkinen, H.; Vattulainen, I.; Akola, J. *J. Phys. Chem. C* **2012**, *116*, 9805-9815.
- (S68) Ahn, Y.; Saha, J. K.; Schatz, G. C.; Jang, J. K. *J. Phys. Chem. C* **2011**, *115*, 10668-10674.
- (S69) Awarke, A.; Wittler, M.; Pischinger, S.; Bockstette, J. *J. Electrochem. Soc.* **2012**, *159*, A798-A808.
- (S70) Lee, O. S.; Cho, V. Y.; Schatz, G. C. *J. Phys. Chem. C* **2012**, *116*, 7000-7005.
- (S71) Nadler, R.; Sanz, J. F. *J. Mol. Model.* **2012**, *18*, 2433-2442.

- (S72) Nadler, R.; Sanz, J. F. *J. Chem. Phys.* **2012**, *137*, 114709.
- (S73) Kim, H. J.; Smit, B.; Jang, J. K. *J. Phys. Chem. C* **2012**, *116*, 21923-32931.
- (S74) Barone, V.; Casarin, M.; Forrer, D.; Monti, S.; Prampolini, G. *J. Phys. Chem. C* **2011**, *115*, 18434-18444.
- (S75) Toth, R.; Voorn, D. J.; Handgraaf, J. W.; Fraaije, J. G. E. M.; Fermeglia, M.; Pricl, S.; Posocco, P. *Macromolecules* **2009**, *42*, 8260-8270.
- (S76) Piscitelli, F.; Posocco, P.; Toth, R.; Fermeglia, M.; Pricl, S.; Mensitieri, G.; Lavorgna, M. *J. Colloid Interface Sci.* **2010**, *351*, 108-115.
- (S77) Cummings, P. T.; Docherty, H.; Iacovella, C. R.; Singh, J. K. *AIChE Journal* **2010**, *56*, 842-848.
- (S78) Docherty, H.; Cummings, P. T. *Soft Matter* **2010**, *6*, 1640-1643.
- (S79) Srivastava, R.; Docherty, H.; Singh, J. K.; Cummings, P. T. *J. Phys. Chem. C* **2011**, *115*, 12448-12457.
- (S80) Srivastava, R.; Singh, J. K.; Cummings, P. T. *J. Phys. Chem. C* **2012**, *116*, 17594-17603.
- (S81) Drummy, L. F.; Jones, S. E.; Pandey, R. B.; Farmer, B. L.; Vaia, R. A.; Naik, R. R. *ACS Appl. Mater. Interf.* **2010**, *2*, 1492-1498.
- (S82) Mathew, D. C.; Luthey-Schulten, Z. *Orig. Life Evol. Biosph.* **2010**, *40*, 303-317.
- (S83) Voora, V. K.; Saidi, W. A.; Jordan, K. D. *J. Phys. Chem. A* **2011**, *115*, 9695-9703.
- (S84) Wallis, P. J.; Chaffee, A. L.; Gates, W. P.; Patti, A. F.; Scott, J. L. *Langmuir* **2010**, *26*, 4258-4265.
- (S85) Sainz-Diaz, C. I.; Francisco-Marquez, M.; Vivier-Bunge, A. *Environmental Chemistry* **2011**, *8*, 429-440.
- (S86) Xu, W.; Zeng, Q. H.; Yu, A. B. *Polymer* **2012**, *53*, 3735-3740.

(S87) Das, J.; Eun, C. S.; Perkin, S.; Berkowitz, M. L. *Langmuir* **2011**, *27*, 11737-11741.